A Tomographic Measurement Technique for Irradiated Nuclear Fuel Assemblies

BY

STAFFAN JACOBSSON SVÄRD

Dissertation presented at Uppsala University to be publicly examined in Häggsalen, Ångströmlaboratoriet, Uppsala, Friday, May 14, 2004 at 09:30 for the degree of Doctor of Philosophy. The examination will be conducted in English.

Abstract
Jacobsson Svärd, S. 2004. A Tomographic Measurement Technique for Irradiated Nuclear Fuel Assemblies. Acta Universitatis Upsaliensis. *Comprehensive Summaries of Uppsala Dissertations from the Faculty of Science and Technology* 967. 85 pp. Uppsala. ISBN 91-554-5944-7

The fuel assemblies used at the Swedish nuclear power plants contain typically between 100 and 300 fuel rods. An experimental technique has been demanded for determining the relative activities of specific isotopes in individual fuel rods without dismantling the assemblies. The purpose is to validate production codes, which requires an experimental relative accuracy of <2 % (1 σ).

Therefore, a new, non-destructive tomographic measurement technique for irradiated nuclear fuel assemblies has been developed. The technique includes two main steps: (1) the gamma-ray flux distribution around the assembly is recorded, and (2) the interior gamma-ray source distribution in the assembly is reconstructed. The use of detailed gamma-ray transport calculations in the reconstruction procedure enables accurate determination of the relative rod-by-rod source distribution.

To investigate the accuracy achievable, laboratory equipment has been constructed, including a fuel model with a well-known distribution of ^{137}Cs. Furthermore, an instrument has been constructed and built for in-pool measurements on irradiated fuel assemblies at nuclear power plants.

Using the laboratory equipment, a relative accuracy of 1.2 % was obtained (1 σ). The measurements on irradiated fuel resulted in a repeatability of 0.8 %, showing the accuracy that can be achieved using this instrument. The agreement between rod-by-rod data obtained in calculations using the POLCA–7 production code and measured data was 3.1 % (1 σ).

Additionally, there is a safeguards interest in the tomographic technique for verifying that no fissile material has been diverted from fuel assemblies, i.e. that no fuel rods have been removed or replaced. The applicability has been demonstrated in a measurement on a spent fuel assembly. Furthermore, detection of both the removal of a rod as well as the replacement with a non-active rod has been investigated in detail and quantitatively established using the laboratory equipment.

Keywords: tomography, nuclear fuel, SPECT, core physics, validation, pin power, safeguards, partial-defect verification

Staffan Jacobsson Svärd, Department of Radiation Sciences, Box 535, Uppsala University, SE-75121 Uppsala, Sweden

To my wife,

Gunilla

List of Papers

This thesis is based on the following papers, which are referred to in the text with their roman numerals:

I   Jacobsson, S., Andersson, C., Håkansson, A., Bäcklin, A., A Tomographic Method for Verification of the Integrity of Spent Nuclear Fuel Assemblies - I: Simulation Studies, *Nuclear Technology*, 135(2), pp. 131-145 (2001).

II   Jacobsson, S., Håkansson, A., Jansson, P., Bäcklin, A. A Tomographic Method for Verification of the Integrity of Spent Nuclear Fuel Assemblies - II: Experimental Investigation, *Nuclear Technology*, 135(2), pp. 146-153 (2001).

III   Jacobsson Svärd, S., Håkansson, A., Bäcklin, A., Jansson, P., Osifo, O., Willman, C., Tomography for partial-defect verification – experiences from measurements using different devices.
        Submitted to the *ESARDA Bulletin*.

IV   Jansson, P., Jacobsson Svärd, S., Håkansson, A., Bäcklin, A. A Device for Non-destructive Experimental Determination of the Power Distribution in Nuclear Fuel Assemblies
        Submitted to *Nuclear Science and Engineering*.

V   Jacobsson Svärd, S., Håkansson, A., Bäcklin, A., Osifo, O., Willman, C., Jansson, P. Non-destructive Experimental Determination of the Pin-power Distribution in Nuclear Fuel Assemblies.
        Submitted to *Nuclear Technology*.

Contents

Abbreviations

ADC	Analog-to-digital converter
ART	Algebraic Reconstruction Technique. An iteration scheme used in algebraic tomographic reconstructions.
ASIRT	Additive Simultaneous Iterative Reconstruction Technique. An iteration scheme used in algebraic tomographic reconstructions.
b	Barn. A unit for cross section of nuclear interaction. Cross section can be interpreted in terms of probability for interaction.
BGO	Bismuth germanate ($Bi_4Ge_3O_{12}$). A scintillation material for gamma-ray detection.
BU	Burnup. The total amount of energy produced in nuclear fuel. Power integrated over time. BU is often expressed in the unit GWd/tU.
BWR	Boiling water reactor.
CLAB	Swedish interim storage for spent nuclear fuel (Centralt mellanlager för använt kärnbränsle).
Ge	Germanium. A semi-conducting element suitable for gamma-ray detection.
GW	Gigawatt. A power unit. 1 GW = 10^9 W = 10^9 J/s
GW(e)	Gigawatt electric power.
GWd	Gigawatt days. A unit for energy. The energy produced (or consumed) by 1 GW power during 24 h. 1 GWd = $2.4 \cdot 10^7$ kWh.
GWd/tU	Gigawatt days per metric ton of uranium that was initially present in the fuel. A unit for burnup (BU).
GWh	Gigawatt hours. A unit for energy. The energy produced (or consumed) by 1 GW during one hour. 1 GWh = 10^6 kWh.
keV	Kilo electron volt. A unit of photon energy. 1 keV is

	equal to the kinetic energy of an electron that is accelerated over a potential of 1 kV.
kGy	Kilogray. A unit of radiation dose. 1 kGy corresponds to an absorbed radiation energy per mass unit of 1000 J/kg.
LWR	Light water reactor, includes BWRs and PWRs.
MCA	Multi-channel analyzer
ML	Maximum Likelihood. An expression for techniques to extract a data set for which the statistical probability is maximized. ML techniques may be applied in tomographic reconstructions.
NIM	Nuclear Instrumentation Module. A standard for electronics equipment in nuclear data-acquisition systems.
NPP	Nuclear power plant.
PM tube	Photo-multiplier tube. A device used in connection with gamma-ray detectors of the scintillation type.
PWR	Pressurized water reactor.
SPECT	Single photon emission computed tomography

1 Introduction

This thesis consists of a comprehensive summary, based on five scientific papers. It describes a newly developed non-destructive tomographic measurement technique and its application in measurements on nuclear fuel assemblies. Although the technique can be applied generally, the thesis is focused on the fuel types and the operating conditions of the Swedish nuclear power industry.

1.1 Nuclear power

Nuclear power is the source of about 17 % of the electric energy produced in the world. As of January 1, 2003, there were 441 nuclear power plants (NPPs) in operation with a total net installed capacity of 359 GW(e). Furthermore, there were 32 NPPs under construction. During 2002, the world total nuclear electricity production was about $2.6 \cdot 10^6$ GWh [1]. In Sweden, there are currently eleven NPPs in operation, producing about half of the electric energy in the country.

The basis for nuclear power is the fission reaction, i.e. the process where a heavy atomic nucleus, such as uranium, splits into lighter nuclei, called fission products. A large amount of energy is released in this process. If all nuclei in 1 g uranium are subject to fission, an energy of about 24 000 kWh is released, which is sufficient to heat a typical house in Sweden during one year. For comparison, production of the same amount of energy by combustion techniques requires about 3 m^3 or 2.5 metric tons of oil.

In a nuclear power reactor, the fission process is used for producing energy by controlling a self-sustained chain reaction. Such a reaction can be obtained because of the ability of neutrons to induce fission and because typically 2-3 neutrons are emitted in the fission of one heavy nucleus.

1.1.1 Types of nuclear fuel used in Sweden

All eleven nuclear power reactors in operation in Sweden are of the LWR type, where the reactor core contains a mix of fuel and water. Eight of the reactors are boiling water reactors (BWR) and three are pressurized water reactors (PWR). In the BWR reactors, the water in the core is heated so that boiling occurs. The steam that is generated is lead through a turbine, which

is connected to a generator so that electric power is produced. In the PWR reactors, no boiling occurs in the core; instead steam is generated in a heat exchanger. Electric energy can then be produced using the steam the same way as in a BWR reactor.

The water in the LWR cores is thus required in the conversion of the energy released in the fission process to electric energy. It is also required for cooling the fuel. Furthermore, the water is required for slowing down, or moderating, neutrons released in the fission process from fast to thermal energy, i.e. an energy where the neutrons are in thermal equilibrium with the surrounding material. At that energy, the probability for neutron-induced fission in a fissile nucleus is considerably larger than at higher energies. Accordingly, the moderation of neutrons is required to obtain a self-sustained fission chain reaction in the core.

Consequently, the fuel in LWR reactors is designed to obtain an optimized uranium-to-water ratio. This is done by stacking the UO_2 pellets in zircaloy[1] tubes of about 4 m length with a diameter of about 10 mm. These tubes, or fuel rods, are mounted in assemblies with in the order of 100-300 rods in each. The two main types of fuel assemblies used in Sweden are:

- BWR assemblies. This type of assembly contains about 100 fuel rods. Furthermore, a fuel channel surrounds the rods in order to lead boiling water through the assembly. The weight of a BWR assembly is about 200 kg.
- PWR assemblies. This type of assembly typically contains 200-300 rods. No fuel channel is required. The weight is about 400 kg.

Both fuel types may also contain empty zircaloy tubes, so called water channels, in which water can be transported. In the case of PWR fuel, empty zircaloy tubes can also be used for in-core instrumentation. The two types of assemblies are illustrated in Figure 1.1.

---

[1] An alloy based on Zirconium.
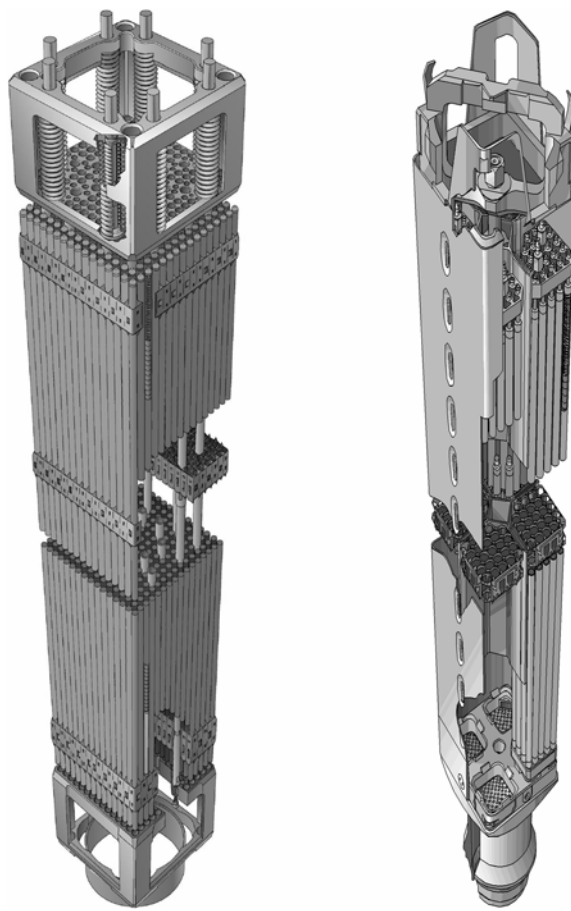
Figure 1.1. Illustrations of fuel assemblies for PWR reactors (left) and for BWR reactors (right). Reproduced by courtesy of Westinghouse Electric Sweden AB.

The size of the axial cross section is about $210\text{x}210 \text{ mm}^2$ for PWR assemblies and about $140\text{x}140 \text{ mm}^2$ for BWR assemblies. Examples of cross sections are illustrated in Figure 1.2 and Figure 1.3, respectively. In these figures, UO_2 material is illustrated using gray shade.
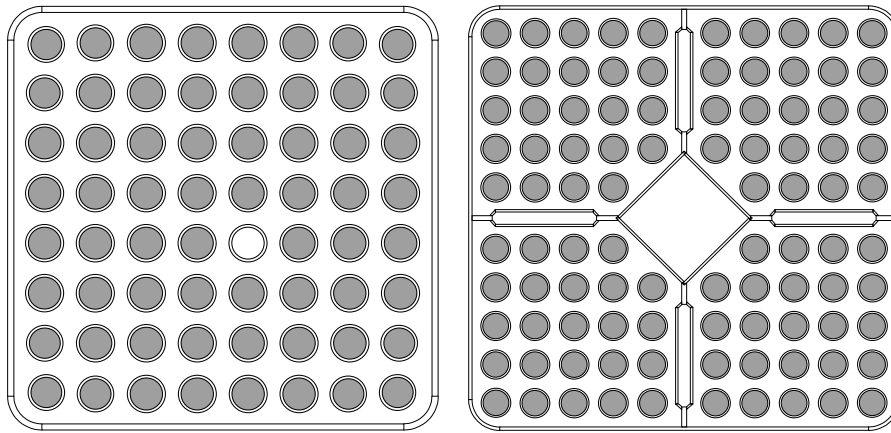
Figure 1.2. The cross sections of two BWR fuel assemblies, one of the 8x8 type, with 63 rods and one water channel (left) and one of the SVEA-96S type, with 96 rods divided into four sub-bundles (right). The UO_2 material is represented using gray shade. Fuel channels surround the fuel bundles.
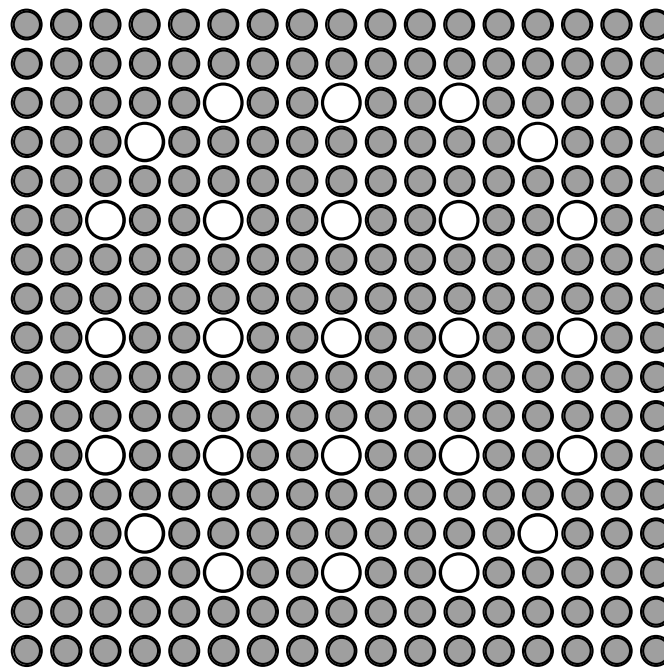
Figure 1.3. The cross section of a PWR assembly of the 17x17 type, with 264 fuel rods and 25 water channels. The UO_2 material is represented using gray shade. No fuel channel surrounds the fuel bundle.

1.1.2 The Swedish nuclear fuel cycle

The use of nuclear fuel in Sweden is based on a once-through cycle; meaning that the spent fuel will not be reprocessed. The Swedish nuclear fuel cycle is schematically illustrated in Figure 1.4.
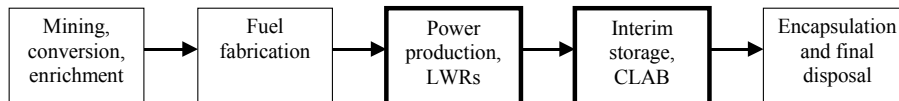
Figure 1.4. The "once-through" nuclear fuel cycle adopted in Sweden. Measurements described in this thesis have been performed on fuel assemblies at an LWR plant and at the interim storage facility, CLAB[2]. However, the technique is also relevant prior to final disposal, as discussed in section 2.1.

The basic element used in nuclear fuel is uranium. There are three natural isotopes of uranium with abundances according to Table 1.1.

Table 1.1: *Isotopic abundance of natural uranium.*

Isotope	Abundance [%]
^{238}U	99.2745
^{235}U	0.72
^{234}U	0.0055

Of these isotopes, only ^{235}U is fissile, i.e. it can undergo fission by capturing a thermal neutron. Accordingly, nuclear reactors of the LWR types require the fuel to be enriched in ^{235}U, typically to a content of between 2 % and 5 %, so called low-enriched fuel.

In the fuel fabrication, the enriched uranium is converted to uranium dioxide, UO_2, which is sintered to fuel pellets. The pellets are stacked in tubes, which are mounted in assemblies. The properties of LWR fuel assemblies are described in section 1.1.1.

The Swedish LWRs are operated in power cycles of about one year. Each irradiation period is followed by a revision shutdown period of typically 2-4 weeks. A fuel assembly is irradiated in the core for an approximate period of about five power cycles. Consequently, about 20 % of the assemblies in the core are exchanged with fresh ones every year. This is done during the revision shutdown period.

When the fuel has been removed from the core, it is moved to CLAB, in Oskarshamn. After a cooling time of about 30 years, it is planned that the fuel will be encapsulated and stored in a deep geological repository [2].

---

[2] Centralt mellanlager för använt kärnbränsle. Situated in Oskarshamn.

In this thesis, the following definitions are used for fuel at different stages of the fuel cycle:

- Fresh fuel. Fabricated fuel that has not yet come into operation.
- Irradiated fuel. Fuel that has been used in power production. The irradiation time in the reactor core may have been long or short. It may also be recent or remote in time.
- Spent fuel. Irradiated fuel that will not be used in the reactor core again.

The measurement technique described in this thesis is intended for irradiated and spent fuel. Sites where the measurement technique has been applied are indicated in Figure 1.4.

1.1.3 Safeguards

The fissile material in nuclear fuel may also be used in nuclear weapons. The two isotopes mostly discussed in this context are ^{235}U and ^{239}Pu, of which the latter is produced in nuclear reactors. It is very difficult to extract these isotopes from the fuel. Still, it is possible and for that reason international efforts are made to ensure that fissile material is used according to international agreements. These activities are called safeguards.

The organization responsible for the safeguards assessments is the International Atomic Energy Agency, IAEA [3]. The IAEA was set up in 1957 within the United Nations with the purpose to promote safe, secure and peaceful use of nuclear technologies worldwide. The IAEA cooperates with regional authorities, such as Euratom in Europe, and national authorities, such as the Swedish Nuclear Power Inspectorate, SKI.

The safeguards authorities perform inspections of nuclear facilities under international safeguards agreements, such as the global Treaty on the Non-Proliferation of Nuclear Weapons (NPT). There is a continuous chain of control and surveillance of the fissile material, from the excavation of uranium ores to final repository or reprocessing.

1.2 Tomography

The measurement technique described in this thesis is a tomographic method. The origin of the word tomography is from the Greek words *to'mos*, which means slice or section, and *-graphi'a*, which means draw. In more technical terms, tomography means techniques to create sectional images of the interior of objects by performing external measurements.

Tomography is widely used in medicine, where images of inner sections of the human body are obtained. There are various tomographic techniques,

in which different properties of the body are measured and illustrated in cross-sectional images. Some examples are X-ray computed tomography (CT), single photon emission computed tomography (SPECT), positron emission tomography (PET), ultrasonic tomography and magnetic resonance tomography (MR). See e.g. refs. [4] and [5].

There are also a variety of industrial applications of tomographic techniques. In the nuclear power industry, the CT technique has e.g. been applied on individual fuel rods and also on fuel assemblies [6]. Using this technique, images of the density distribution in a section of the object can be obtained with high spatial resolution. Furthermore, the SPECT technique has been applied on barrels with nuclear material [7] and on individual fuel rods [8, 9, 10]. Using this technique, images of the interior distribution of radioactive isotopes are obtained.

In this thesis, the SPECT technique has been applied on nuclear fuel assemblies. Here, the gamma-ray flux distribution around a fuel assembly is recorded and, using the recorded information in computer-aided calculations, images of the interior gamma-ray source distribution in a section of the assembly can be reconstructed. This application has been demonstrated earlier [11, 12]. The purpose of the present technique is to obtain accurate quantitative values of the relative rod-by-rod content of the gamma-ray source. The technique therefore involves detailed physical modeling, which is elaborately described in section 4. Two applications of the technique have been demonstrated in section 6 and 7.

2 Scope of the thesis

Although nuclear power is a mature technology, a lot of research and development is still performed and improvements are still made. Two areas have been identified where continued progress may be offered by using new or improved measurement techniques:

- There is a request for new techniques for survey and control of nuclear waste for the purpose of safeguards, see section 1.1.3.
- There is a strong desire to use the fuel more efficiently and to limit the amount of nuclear waste generated. Extended use of the fuel requires better knowledge of the fuel behavior in the core, which in turn requires experimental data.

Within the scope of this thesis, a technique for tomographic measurements on nuclear fuel assemblies has been developed and its applicability for these two purposes has been investigated.

2.1 Partial-defect verification

An important safeguards activity is verification of fuel integrity, i.e. verification of the completeness of fuel rods in a fuel assembly versus operator-declared data. In the IAEA Safeguards Criteria [13], the term defect is used, defined as the "difference between the declared amount of nuclear material … and the actual amount present". Three levels of defect are specified:

1. Gross defect. All nuclear material is missing, i.e. all fuel rods in an assembly are missing or replaced.
2. Partial defect. A fraction of the declared amount of nuclear material is missing. In connection to difficult-to-access storage, such as final repository, it is defined that "the partial defect test should assure that at least half of the fuel pins are present in each assembly" [13]. In this thesis, a missing amount of nuclear material corresponding to a single rod is referred to as "partial defect on the single rod level".
3. Bias defect. This definition refers to "testing using the most precise measurement method available" [13].

16

Preferably, safeguards inspections should be performed using non-destructive techniques, NDA. For verification of gross defect, there are several NDA techniques, which have been approved by the IAEA [14]. However, so far no NDA instrument has been approved by the IAEA for the purpose of partial or bias defect verification [15].

Two NDA techniques that are considered for the purpose of partial-defect verification of spent nuclear fuel assemblies are:

- The detection of Cherenkov radiation, e.g. using an instrument called the Digital Cherenkov Viewing Device (DCVD) [16].
- The detection of neutron radiation [17]. Investigations have e.g. been performed using an instrument called the Enhanced Fork Detector Irradiated Fuel Measuring System (EFDET) for combined neutron and gamma-ray detection [18].

The usefulness of these techniques for partial-defect verification has so far not been settled.

Recently, tomographic techniques have been acknowledged in the safeguards community as a possible means for experimental verification of partial defect, even on the single rod level. In Sweden and Finland, the discussions relate to safeguards measurements on spent fuel in connection to the planned final-repository facilities [19, 20].

In this thesis, a tomographic technique for experimental verification of partial defect has been developed. Instrumentation for in-pool measurements has been constructed and the applicability of the technique has been demonstrated. This is covered in Papers I, II and III. The main purpose has been to investigate the applicability of a stationary device for partial-defect verification at the final-repository facility planned for in Sweden.

An alternative tomographic technique, also developed for the purpose of partial-defect verification, is described in refs. [11] and [12]. In this case, the instrumentation applied has mainly been intended for inspection use.

2.2 Validation of production codes for core simulation

At the nuclear power plants, regular measurements are performed to follow up the behavior of the reactor core. The neutron flux distribution in the core is monitored during power production and measurements are performed on individual fuel assemblies during revision shutdown periods.

However, safe and efficient operation of the reactor core relies to a large extent on extensive computer-aided calculations, which are performed using production codes for core simulation. In these codes, the complete core physics, including all nuclear processes, as well as the thermo-hydraulics of the moderator, are considered.

There is a general interest in the nuclear-power community of validating the production codes, e.g. with respect to the power distribution in the core. Because modern production codes perform calculations on the fuel rod level, a need for experimental data on individual fuel rods has been recognized. New fuel designs and more flexible reactor operation attract additional interest to this type of experimental validation. Examples of positions in the core that may be difficult to model are regions near the end of part-length rods and partially inserted control rods.

An international project has been carried out in order to benchmark the calculation accuracy of production codes [21]. Ten institutions from eight countries simulated a model core, using more than fifteen calculation schemes. The averaged standard deviation in the determination of power in UO_2 fuel rods was 3.5 %. The largest standard deviation between the codes in any UO_2 rod was 15.7 %.

In addition to the consistency of different calculation schemes discussed above, practical factors can adversely affect the accuracy of the calculated power distribution. An example of such a factor in BWR fuel is channel bow, i.e. the tendency of the fuel channel, which surrounds the BWR assemblies, to bend due to the neutron flux. This will affect the power in individual fuel rods due to local changes in the thickness of the water gap between adjacent assemblies. Simulations described in refs. [22] and [23] show that the relative pin power in the most affected rods can change with about 2-4 % per mm channel bow and the bow can occur with a magnitude of several mm. In addition, individual pins may be dislocated, both in BWR and PWR fuel.

The established way of experimentally determining the pin-power distribution in irradiated fuel is to measure the distribution of the fission product ^{140}Ba, see section 3.1.1. In the method practiced so far, the bundle is disassembled and gamma scanning of individual fuel rods is performed [24, 25, 26, 27]. In BWR fuel, the fuel channel is also removed. However, this technique is time-consuming, limiting a measuring campaign to typically 30-60 rods. Therefore, it is not very cost-effective. Furthermore, it raises both safety- and safeguards concerns.

The tomographic technique described in this thesis has been developed to offer an alternative way to perform experimental determination of the pin-power distribution. It is attractive because it does neither require the fuel to be disassembled, nor does it require the fuel channel to be removed from BWR assemblies. In this project, an experimental accuracy below 2 % (1 σ) in the determination of the pin-by-pin content of ^{140}Ba was set as a desirable goal to experimentally validate production codes. Instrumentation for in-pool measurements has been constructed and the technique has been demonstrated on BWR fuel. This is accounted for in Papers IV and V.

3 Properties of irradiated nuclear fuel

The core in a typical Swedish nuclear power reactor contains about 500 fuel assemblies, see section 1.1.1. During operation of such a reactor, a self-sustained fission chain reaction is controlled in the core, induced by a neutron flux of about $10^{14}/(cm^2 \cdot s)$. When the fuel is irradiated in this neutron flux, a variety of nuclear reactions occur. Consequently, the composition of the fuel is altered with time.

A large amount of radioactive fission products are created, with half-lives ranging from less than a second to several decades. Neutron capture and nuclear decay in fission products as well as in heavy nuclei causes further changes to the composition of the fuel.

Altogether, the properties of irradiated fuel gradually change from that of fresh fuel. For example, in fresh fuel, about 92 % of the fission reactions occur in ^{235}U and about 8 % occur in the more abundant nucleus ^{238}U, due to the flux of fast neutrons [24]. During irradiation, the abundance of ^{235}U is reduced while other fissile nuclides, such as ^{239}Pu and ^{241}Pu, are created. At the end of the irradiation, after about five power cycles, these additional fissile nuclei may contribute to the fission rate with about 60 % and 20 %, respectively [24]. The contribution from ^{235}U will then have decreased to about 10 % while the contribution from ^{238}U remains at about 10 %.

In addition, several of the fission products strongly absorb neutrons, which has to be taken in consideration in operating the reactor. Accordingly, it is of vital importance to keep track of the fuel composition in order to predict the behavior of the fuel in the reactor core.

Some parameters of importance for characterizing irradiated fuel are:

- Initial enrichment. (The initial content of ^{235}U, see section 1.1.2.)
- Burnup (BU). The total amount of energy produced in the fuel, which depends on the spatial distribution of the thermal power and its variation in time, also called the power history. BU is usually expressed as energy per initial mass of uranium, e.g. GWd/tU.
- Cooling time (CT). The time since the latest power cycle ended.

It possible to obtain information about these fuel parameters, and others, by measuring radiation emitted from radioactive nuclei present in irradiated fuel [28, 29].

3.1 Irradiated fuel assemblies as a gamma radiation source

For the tomographic measurements described in this thesis, gamma-emitting isotopes are of particular interest. However, only isotopes with a half-life longer than a few days can be utilized because the measurements cannot be performed in-core. Furthermore, the isotopes should emit gamma radiation of sufficient energy to escape from the assemblies. The higher the gamma-ray energy, the more information can be obtained from the inner sections. At 662 keV, only about 4 % of the radiation from a central fuel rod in a BWR assembly can escape the fuel assembly, even when emitted perpendicularly to the assembly axis. Because of the larger size of PWR assemblies, as described in section 1.1.1, the corresponding figure for PWR fuel is only about 1 %. At 1274 keV the escape fraction is a factor of about 5 higher.

Depending on the cooling time of the fuel, different isotopes may be of relevance for a specific measurement. This depends on their concentrations, half-lives and decay modes. Some isotopes of interest are listed in Table 3.1. Here, only gamma energies higher than 600 keV have been considered.

Table 3.1: *Isotopes that can be used in tomographic measurements on nuclear fuel assemblies.*

Isotope	Gamma energies [keV]	Half-life	Relevant CT
^{140}Ba (^{140}La)	1596	12.8 d	<50 d
^{95}Zr (^{95}Nb)	724, 757, 766	64 d	30 d – 0.5 y
^{144}Ce (^{144}Pr)	696, 2186	284 d	0.3 – 2 y
^{134}Cs	605, 796	2.1 y	1 – 10 y
^{154}Eu	1274	8.5 y	2 – 30 y
^{137}Cs	662	30 y	2 – 100 y

Another property that may affect the measurements of some of the listed isotopes is migration, i.e. the relocation of elements in the fuel matrix. In particular, volatile elements are sensitive to migration. The gamma radiation from isotopes that tend to migrate towards the periphery of the rods, such as ^{137}Cs, escape the rods to a larger extent than the radiation from isotopes that do not migrate, such as ^{154}Eu [28]. However, in this case, it is considered that migration can be taken into account in the tomographic analysis procedure, as discussed in section 4.2.5.

In the work accounted for in this thesis, radiation emitted in the decay of ^{140}Ba, ^{154}Eu and ^{137}Cs has been utilized.

3.1.1 ^{140}Ba

As mentioned in section 2.2, radiation from ^{140}Ba may be used to study the thermal power distribution in fuel assemblies. However this utilization of ^{140}Ba requires knowledge of its production in the reactor core. The main production paths of ^{140}Ba are presented in Figure 3.1.
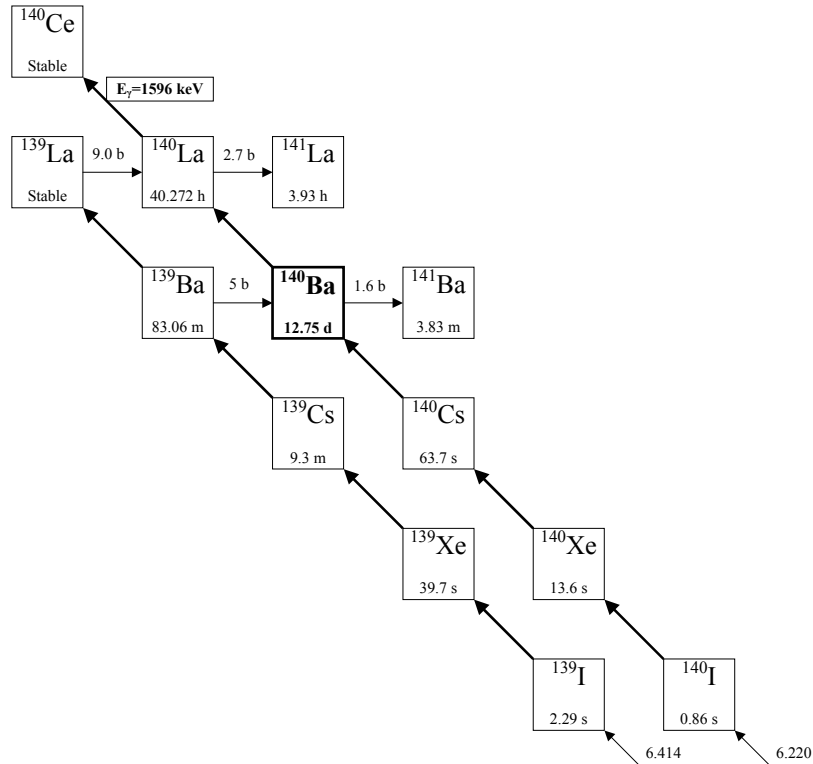
Figure 3.1. Production and decay of ^{140}Ba. Beta decay is illustrated with diagonal arrows and neutron capture with horizontal arrows. Half-lives and cross sections for thermal neutron capture are taken from ref. [30]. Cumulative chain yields for each mass chain are presented for fission induced by thermal neutrons in ^{235}U, as given in ref. [31].

The production of ^{140}Ba is dominated by direct fission in mass chain 140 in combination with repeated beta decay. An alternative production path is through neutron capture in ^{139}Ba. However, this production is, in practice, negligible, because the half-life of ^{139}Ba is relatively short (83 minutes) and the neutron capture cross section is small (5 b). On the other hand, ^{140}Ba itself has a cross section for neutron capture of 1.6 b, which may introduce a small loss at high neutron flux, i.e. high thermal power.

The production mode and the relatively short half-life of 12.8 days have two main implications for measurements of the ^{140}Ba radiation:

21

(1) The abundance of ^{140}Ba in a fuel rod will be strongly correlated to the thermal power during the last few weeks before outage.
(2) The measurements have to take place shortly after fuel outage.

It should be noted that the 1596 keV gamma radiation that is measured to determine the distribution of ^{140}Ba is emitted in the decay of the more short-lived daughter ^{140}La, see Figure 3.1. Because ^{140}La is also to some extent produced through neutron capture in the stable isotope ^{139}La, it is important to wait until the ratio ^{140}La/^{140}Ba approaches equilibrium to avoid a time-dependent component. Measurements should therefore not be started until 10-15 days after outage.

It should also be noted that the cumulative yield of ^{140}Ba is different for fission in different mother nuclei, as accounted for in Table 3.2.

Table 3.2: *Cumulative yield of ^{140}Ba in thermal fission of nuclei dominating in LWR operation. From ref. [32].*

Mother nucleus	Cumulative yield of ^{140}Ba (nuclei per 100 fissions)
^{235}U	6.21
^{239}Pu	5.35
^{241}Pu	5.77
^{238}U	5.82[a)]

a) Yield in fission induced by fast neutrons.

Because fission occurs more frequently in ^{239}Pu and ^{241}Pu with increasing burnup, the yield of ^{140}Ba will decrease with burnup [24].

Modern production codes for core simulation calculate the distribution of ^{140}Ba in the fuel. The dominating input in this calculation is the power distribution history. Accordingly, a valid benchmark of the calculated power distribution can be obtained by comparing measured and calculated distributions of ^{140}Ba [24].

3.1.2 ^{137}Cs

In irradiated fuel with a few years cooling time, the gamma-ray emission is dominated by ^{137}Cs, which has a half-life of about 30 years.

The production of ^{137}Cs is illustrated in Figure 3.2. It is dominated by direct fission in mass chain 136 in combination with repeated beta decay. An alternative production path is neutron capture in the stable isotope ^{136}Xe. However, the neutron capture cross section is small (0.26 b) and, furthermore, the loss of ^{137}Cs through neutron capture is about equally large (0.25 b).
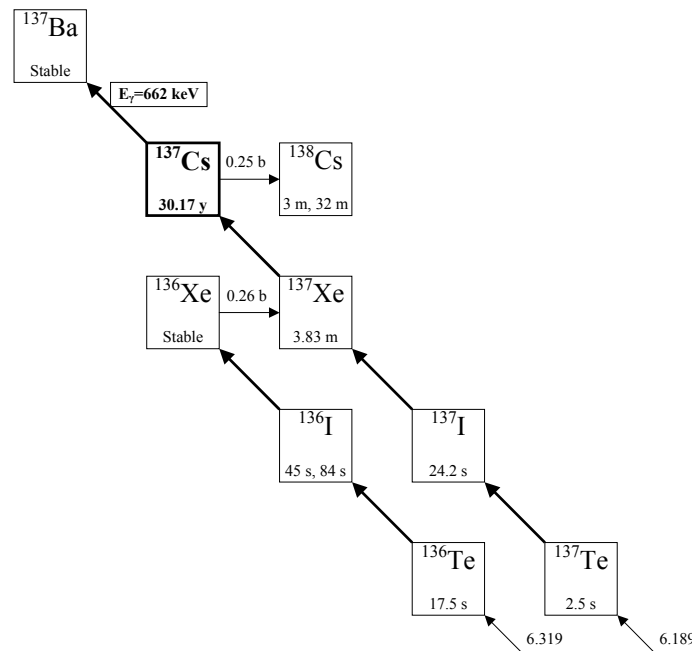
Figure 3.2. Production and decay of ^{137}Cs. Beta decay is illustrated with diagonal arrows and neutron capture with horizontal arrows. Half-lives and cross sections for thermal neutron capture are taken from ref. [30]. Cumulative chain yields for each mass chain are presented for fission induced by thermal neutrons in ^{235}U, as given in ref. [31].

The combination of the relatively long half-life and the production through direct fission implies that the abundance of ^{137}Cs is strongly correlated to burnup. The decay during the irradiation period will be insignificant. Furthermore, measurements can take place several decades after outage.

3.1.3 ^{154}Eu

The production of ^{154}Eu in a nuclear reactor is relatively complicated, as presented e.g. in ref. [33]. However, it can be noted that by measuring the gamma radiation from ^{154}Eu in combination with ^{134}Cs and/or ^{137}Cs, fuel parameters such as burnup and cooling time can be determined [29].

   In the measurements described in section 6.3, the rod-by-rod distribution of ^{154}Eu in a fuel assembly was determined. The activity values obtained were interpreted in terms of the presence of each rod. A possible development of this technique is to determine fuel parameters for each fuel rod in an assembly by analyzing ^{154}Eu in combination with ^{134}Cs and/or ^{137}Cs.

4 Method

The measurement technique that has been applied in this work is called Single Photon Emission Computed Tomography (SPECT). The high flux of gamma radiation emitted from an irradiated nuclear fuel assembly is utilized. The measurement procedure involves two main steps:

1. The gamma-flux distribution is recorded using one or several detectors in a large number of positions relative to the measured assembly.
2. The information collected is used to reconstruct the assembly's interior gamma-ray source distribution.

The first step requires a gamma-radiation detection system that is capable of spatial selection and quantification of the gamma flux. The latter step requires adequate reconstruction algorithms and computational resources.

4.1 Recording of the gamma-ray flux distribution

A basic requirement of a device for tomographic measurements is the ability to record the gamma radiation in a large number of positions (typically 1 000-10 000) relative to the measured object. In each position, gamma-ray detectors are used for collecting information about the gamma flux. Because irradiated nuclear fuel assemblies contain a variety of radioactive isotopes, the data-acquisition system should be able to distinguish between the radiation of interest and other radiation.

A schematic illustration of the tomographic data-collection procedure is presented in Figure 4.1. Here, the gamma-flux distribution is recorded at a selected axial level of a nuclear fuel assembly. The assembly is fixed and the instrumentation performs all required movements.
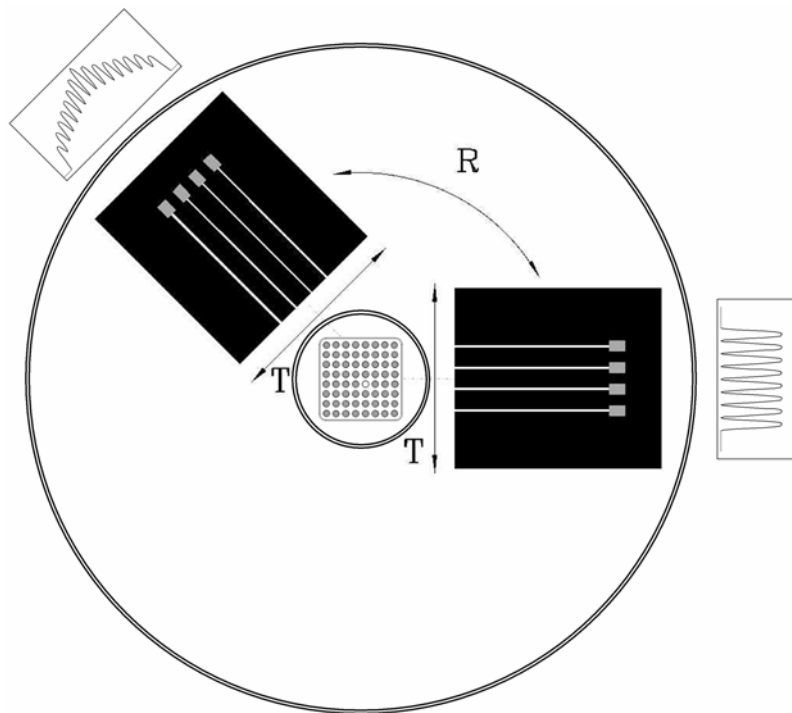
Figure 4.1. A schematic illustration of the data-collection procedure. A collimator package including four detectors is rotated (R) and translated (T) to record the distribution of the radiation field in various positions relative to a fuel assembly of the BWR 8x8 type. Two angular positions of the collimator package are indicated and corresponding gamma-ray intensity profiles are illustrated.

The gamma-ray detectors are fitted with a collimator system in order to define the section of the object to contribute to the measured gamma-ray intensity in a certain position. The measured intensity in each position will thus contain information from a specified section of the fuel. The spatial resolution of the tomographic reconstructions depends on the dimensions of the collimator slits.

4.2 Tomographic reconstruction

There are two main types of tomographic reconstruction algorithms, analytic and algebraic, see e.g. ref. [5].

The analytic methods are based on a mathematical solution to the problem of how to reconstruct a function from its projections, presented by Johann Radon in 1917. For the purpose of tomographic reconstruction for medical applications, Radon's theory is dominantly utilized using Fourier techniques. Algebraic algorithms, on the other hand, are based on algebraic equation

formalism for finding a solution to a set of unknown image data using measured projection data.

For many medical applications, analytic techniques offer fast and accurate reconstruction. However, for the SPECT measurement technique applied in this thesis, these techniques are considered to suffer from weaknesses in the modeling of the collimation [5]. Furthermore, for objects with strongly non-uniform gamma-ray attenuation, such as nuclear fuel assemblies, difficulties are encountered when attempting to take the attenuation into account. It should be noted that there are techniques for including uniform attenuation, see e.g. ref. [34], and recently a numerical analytic solution for objects with strongly non-uniform attenuation has also been presented [35].

Algebraic reconstruction techniques allow for physical modeling to a larger extent than analytic methods. Umbra and penumbra effects of applied collimation can be modeled in detail, e.g. as accounted for in section 4.2.2. Furthermore, the well-known nominal geometry of a fuel assembly can be utilized for detailed modeling of the gamma-ray attenuation. Another benefit of the algebraic reconstruction technique in this context is its feasibility for extracting numerical values of the gamma-ray source concentration in each fuel rod. In view of the high accuracy desired in the determination of the rod-by-rod gamma-ray source concentration, see section 2.2, an algebraic approach was therefore selected.

4.2.1 The algebraic approach

The reconstructed cross section of the measured object is divided into picture elements, pixels. The fraction of the emitted gamma quanta from a certain pixel reaching the detector in a certain position can be calculated theoretically. This fraction is here called a contribution coefficient. Summation over all pixels, $n \in 1..N$, gives the gamma-ray intensity in the detector in a certain position:

$$I_m = \sum_{n=1}^{N} A_n \cdot w_{mn}$$

Eq. (4.1)

where w_{mn} = the contribution coefficient from pixel n to the detector in position m,
A_n = the gamma-source concentration in pixel n,
I_m = the intensity in measurement position m.

Using measured intensities in a large number of detector positions, $m \in 1..M$, an equation system is obtained:

$$
\begin{pmatrix}
w_{11} & w_{12} & \cdots\cdots\cdots & w_{1N} \\
w_{21} & w_{22} & & w_{2N} \\
\vdots & & \ddots & \\
& & & \\
w_{M1} & w_{M2} & & w_{MN}
\end{pmatrix}
\begin{pmatrix}
A_1 \\
A_2 \\
\vdots \\
\\
A_N
\end{pmatrix}
=
\begin{pmatrix}
I_1 \\
I_2 \\
\vdots \\
\\
I_M
\end{pmatrix}
\qquad \text{Eq. (4.2)}
$$

The equation system is solved for the pixel activities, **A**. In the investigations described here, the number of equations (measurements), M, has been larger than the number of unknown variables (pixels), N.

The contribution coefficients depend on gamma-ray attenuation and geometric conditions. Information about the geometry of the measured object can be used in order to obtain more accurate coefficients, implying better quality of the reconstructions of the gamma-ray source distribution. This is especially important in measurements of objects with highly varying gamma-ray attenuation conditions, such as nuclear fuel assemblies.

Some basic assumptions have been made in this thesis in order to obtain an expression for the contribution coefficients:

- The gamma-ray emission is isotropic.
- Only full-energy transport of mono-energetic gamma rays is considered.
- Elastic scattering is neglected.
- The detector is small and placed relatively far from the object, implying that all gamma rays from a certain point of emission to the detector travel along approximately the same path through the object.

These assumptions are relevant provided that (1) spectroscopic analysis is performed on the detector signals so that events are isolated that correspond to full-energy absorption of a selected gamma-ray energy in the detector, and (2) a measuring geometry is used that fulfill the last assumption.

The third assumption is relevant because the cross section for elastic scattering is small relative to the total cross section at the gamma-ray energies considered here, especially for light materials. For 1596 keV gamma rays in water, elastic scattering accounts for only about 0.04 % of the gamma-ray interaction. However, in UO_2, the corresponding figure is 2.5 %. The contribution from elastic scattering may be taken into consideration in future work.

To a first approximation, each contribution coefficient w_{mn} can be expressed as:

$$w_{mn} = \frac{A_{det,mn}}{4\pi R_{mn}^2} \cdot e^{-\sum_i \mu_i d_{i,mn}}$$

Eq. (4.3)

where $A_{det,mn}$ = the exposed detector area as seen from pixel n when the detector is in position m,

R_{mn} = the distance between pixel n and the detector at position m,

μ_i = the attenuation coefficient of material i,

$d_{i,mn}$ = the travel distance in each material i of a gamma-ray from pixel n to the detector in position m.

The first factor in Eq. (4.3) accounts for the solid angle of the exposed part of the detector, as seen through the collimator slit from pixel n, and the second factor accounts for the gamma-ray absorption in the object. An implementation of this expression in two spatial dimensions was used in Papers I and II.

However, Eq. (4.3) does not take into account any contribution from gamma-ray transmission through the collimator material. Simulations of the experimental geometry accounted for in section 5.5 showed that this contribution is significant; about 16 % of the full-energy 1596 keV gamma rays that reach the detectors had been transmitted through some section of the collimator. Furthermore, accurate implementation requires that three spatial dimensions be considered.

A technique for enhanced modeling of the object and the measurement geometry was therefore developed, resulting in the expression for calculating the contributions coefficients presented in Eq. (4.13), derived in section 4.2.2. This technique was used for calculating the matrix coefficients in the reconstructions accounted for in Papers III-IV.

4.2.2 Derivation of an expression for calculating the matrix coefficients used in algebraic reconstructions

An expression for calculating the coefficient matrix of Eq. (4.2) in detail has been derived, using the basic assumptions accounted for in section 4.2.1.

4.2.2.1 Gamma-ray intensity reaching a detector from a radioactive source without the use of a collimator

The gamma-ray intensity from a radioactive source that reaches a detector can be expressed as:

$$I = \iiint_{x,y,z} a(x,y,z) \cdot \frac{\Omega_{det}(x,y,z)}{4\pi} \cdot e^{-\sum_i \mu_i \cdot d_i(x,y,z)} \cdot dz\, dy\, dx \qquad \text{Eq. (4.4)}$$

where $a(x,y,z)$ = the gamma-source concentration in point (x,y,z),
$\Omega_{det}(x,y,z)$ = the solid angle covered by the detector seen from point (x,y,z),
μ_i = the attenuation coefficient of material i,
d_i = the travel distance in each material i of a gamma-ray from point (x,y,z) to the detector.

The integration in Eq. (4.4) is performed over coordinates (x,y,z) within the volume of the radioactive source.

4.2.2.2   Introduction of an ideal collimator

A collimator is introduced in order to obtain a small and well-defined radiating volume that should contribute to the gamma-ray intensity in a detector at a specific position. The collimator should be made of a highly attenuating material and be equipped with a slit, which governs the properties of the collimator.

In the following discussion, the collimator is considered to be ideal, i.e. the gamma-ray attenuation is (1) infinitely large in the collimator material and (2) negligibly small in the slit. The following properties of the collimator-detector system are assumed:

- Radiation can only reach a detector through the collimator slit.
- The slit area at the detector side of the collimation, here called the exposed detector area, is perpendicular to the slit's main axis.
- The height, h_c, and width, b_c, of the collimator slit are small relative to its length, l_c.

The solid angle covered by the exposed detector area, as seen from a point (x,y,z) in the object, can be expressed as:

$$\Omega_{det}(x,y,z) \approx \frac{A_{det}(x,y,z)}{4\pi R^2(x,y,z)} \qquad \text{Eq. (4.5)}$$

where $A_{det}(x,y,z)$ = the exposed detector area, as seen from point (x,y,z),
$R(x,y,z)$ = the distance from point (x,y,z) to the detector.

4.2.2.3   Reducing the problem to two spatial dimensions

A two-dimensional spatial approach involves the following assumptions:

- The collimator and the detectors are positioned relative to the object in a two-dimensional plane, (x, y), parallel to the collimator slit's main axis, as presented in Figure 4.1.
- The object is spatially uniform along the z-axis, perpendicular to the (x, y)-plane and the source concentration can be represented in two spatial dimensions, so that $a(x,y,z) = a(x,y)$.

The use of the collimator, with properties as described in section 4.2.2.2, justifies the following approximations:

- $d_i(x,y,z) \approx d_i(x,y)$
- $R(x,y,z) \approx R(x,y)$
- $A_{det}(x,y,z) = b(x,y) \cdot h(x,y,z) \approx b(x,y) \cdot h(R,z)$

where $b(x,y)$ = the exposed width of the detector in the x,y-plane seen from point (x,y),
$h(x,y,z)$ = the exposed height of the detector seen from point (x,y,z).

By combining Eq. (4.4) and Eq. (4.5), the following expression is obtained for the gamma-ray intensity reaching the detector:

$$I = \iint_{x,y} a(x,y) \cdot \frac{b(x,y)}{4\pi R^2(x,y)} \cdot e^{-\sum_i \mu_i \cdot d_i(x,y)} \left[\int_z h(R,z)\, dz \right] dy\, dx \qquad \text{Eq. (4.6)}$$

The integral over the z-coordinate can be solved separately. With variables according to Figure 4.2, the integration can be performed according to:

$$\int_z h(R,z) \cdot dz = \int_{z_{min}(R)}^{z_1} h(R,z) \cdot dz + \int_{z_1}^{z_2} h_c \cdot dz + \int_{z_2}^{z_{max}(R)} h(R,z) \cdot dz$$
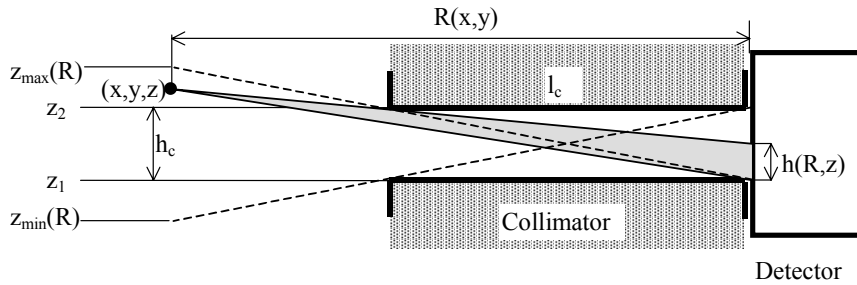
Figure 4.2. Side view of the collimator, illustrating the exposed height of the detector from point (x,y,z).

30

For symmetry reasons this integration can be simplified to:

$$\int_z h(R, z) \cdot dz = h_c^2 + 2 \cdot \int_{z_2}^{z_{max}(R)} h(R, z) \cdot dz$$

Setting $z_2 = 0$ implies:

$$\begin{cases} z_{max}(R) = h_c \cdot \left(\dfrac{R(x, y)}{l_c} - 1 \right) \\ \\ h(R, z) = \dfrac{l_c}{R(x, y) - l_c} \cdot z \qquad \left[z_2 \leq z \leq z_{max}(R) \right] \end{cases}$$

Solving the integral thus leads to:

$$\int_z h(R, z) \cdot dz = h_c^2 \cdot \frac{R(x, y)}{l_c} \qquad\qquad \text{Eq. (4.7)}$$

Inserting Eq. (4.7) into Eq. (4.6) gives the following expression for the gamma-ray intensity reaching the detector:

$$I = \iint_{x, y} a(x, y) \cdot \frac{b(x, y)}{4\pi R^2(x, y)} \cdot e^{-\sum_i \mu_i \cdot d_i(x, y)} \left[h_c^2 \cdot \frac{R(x, y)}{l_c} \right] dy\, dx \qquad \text{Eq. (4.8)}$$

4.2.2.4   Inclusion of gamma-ray transmission through the collimator

Simulations of the experimental geometry accounted for in section 5.5 have shown that about 16 % of the full-energy 1596 keV gamma rays that reaches the detectors have been transmitted through some section of the collimator.

To take into account this relatively large contribution to the measured intensity when calculating the contribution coefficients, the whole detector area that faces the object must be considered, not only the parts exposed through the collimator slit. In order to calculate this contribution, a system of coordinates (x_{det}, y_{det}) is defined for the detector area. As earlier, (x,y,z) denotes coordinates in the object.

The travel distances of gamma rays through different materials i, except for the collimator material, are approximated to be independent of coordinates z, x_{det} and y_{det}, and so is the distance R(x,y) between the point (x,y) and the detector.

Based on these assumptions, $I_{coll}(x,y)$, i.e. the gamma-ray intensity in the detector that is emanating from gamma quanta emitted in a point (x,y), which has been transmitted through some section of the collimator, can be defined as:

31

$$I_{coll}(x,y) = \frac{a(x,y) \cdot e^{-\sum_i \mu_i \cdot d_i(x,y)}}{4\pi R^2(x,y)} \cdot \int_z \left(\iint_{\substack{x_{det} \\ y_{det}|_{d_{coll} \neq 0}}} e^{-\mu_{coll} \cdot d_{coll}(x,y,z,x_{det},y_{det})} dx_{det} dy_{det} \right) \cdot dz$$

It should be noted that integration is only performed over detector coordinates (x_{det}, y_{det}) that imply transmission through the collimator, i.e. $d_{coll} \neq 0$.

The following integral is now defined:

$$w_{coll}(x,y) = \int_z \left(\iint_{\substack{x_{det} \\ y_{det}|_{d_{coll} \neq 0}}} e^{-\mu_{coll} \cdot d_{coll}(x,y,z,x_{det},y_{det})} dx_{det} dy_{det} \right) \cdot dz \qquad \text{Eq. (4.9)}$$

By using Eq. (4.9) in Eq. (4.8), the contribution from the gamma-ray transmission through the collimator material can be accounted for:

$$I = \iint_{x,y} \frac{a(x,y)}{4\pi R^2(x,y)} \cdot e^{-\sum_i \mu_i \cdot d_i(x,y)} \left[b(x,y) \cdot h_c^2 \cdot \frac{R(x,y)}{l_c} + w_{coll}(x,y) \right] dy\, dx \qquad \text{Eq. (4.10)}$$

The factor $w_{coll}(x,y)$ depends only on the gamma-ray attenuation coefficient of the collimator material and the dimensions of the collimator slit and the detector.

In the investigations described in this thesis, separate calculations were performed to determine $w_{coll}(x,y)$ by means of numerical integration. The values obtained were then used in two ways:

1. Values were tabulated for various coordinates.
2. Functions were adapted to the calculated values.

In the former case, the value of $w_{coll}(x,y)$ in a specific coordinate (x,y) could be obtained by interpolation and in the latter case, the adapted functions could be used.

4.2.2.5 Defining the contribution coefficients by introducing a pixel pattern

A pixel pattern is introduced in the (x, y)-plane to describe the gamma-ray source concentration in the object. This involves the assumption that the gamma-ray source concentration in each pixel is homogeneous. The source concentration per unit height in pixel n is denoted A_n, according to:

$$a_n(x, y, z) = \frac{A_n}{S_n} \qquad \text{Eq. (4.11)}$$

where S_n = the area of pixel n in the (x, y)-plane.

Inserting Eq. (4.11) into Eq. (4.10) leads to:

$$I_n = \frac{A_n}{S_n} \iint\limits_{x,y \in n} \frac{1}{4\pi R^2(x, y)} \cdot e^{-\sum_i \mu_i \cdot d_i(x,y)} \left[b(x, y) \cdot h_c^2 \cdot \frac{R(x, y)}{l_c} + w_{coll}(x, y) \right] dy \, dx \qquad \text{Eq. (4.12)}$$

Defining the contribution coefficient w_{mn} according to Eq. (4.1) and using Eq. (4.12) gives the following expression:

$$w_{mn} = \frac{1}{S_n} \cdot \left(\frac{h_c^2}{4\pi l_c} \right) \cdot \iint\limits_{x,y \in n} \frac{1}{R(x, y)} \cdot \left[\frac{l_c}{h_c^2 \cdot R(x, y)} \cdot w_{coll}(x, y) + b(x, y) \right] \cdot e^{-\sum_i \mu_i \cdot d_i(x,y)} \cdot dy dx \qquad \text{Eq. (4.13)}$$

4.2.2.6 Concluding remarks on the derived expression

Assuming $w_{coll}(x,y)$ to be calculated separately, according to section 4.2.2.4, it can be noted that Eq. (4.13) only depends on the cross-sectional geometry in the measurement plane (x,y). The matrix coefficients can be thus obtained by performing numerical integration over the area of each two-dimensional pixel, n, for every detector position, m.

Detailed knowledge of the geometry in two spatial dimensions can be used in order to obtain accurate gamma-ray distances in different materials. This feature leads to the possibility to perform accurate, quantitative tomographic reconstructions even for objects where the gamma-ray attenuation matrix involves strong variations. Furthermore, the positions and shapes of the pixels can be adapted to the cross-sectional geometry of the object.

Finally, it can be noted that Eq. (4.12) and Eq. (4.13) relates to the gamma-ray intensity reaching the detector. The detection efficiency is thus not included in these expressions. Provided that the detector efficiency is taken into account, a tomographic reconstruction performed by solving Eq. (4.2), using Eq. (4.13) for calculating the matrix coefficients, will return the gamma-source concentration per unit height in each pixel.

4.2.3 Solving the algebraic matrix equation

Once the gamma-ray intensities have been recorded and the matrix coefficients have been calculated, there are several techniques to solve the matrix equation Eq. (4.2), see e.g. ref. [5]. In the progress of the work presented here, a few different techniques were utilized [36]. However, in

the investigations accounted for in this thesis, the algebraic reconstruction technique, ART, has been adopted.

Here, the reconstruction procedure is started by setting an initial value, A_0, to all pixels. To be consistent with the measured intensities, this value has been defined as:

$$A_0 = \frac{\sum\limits_m I_m}{\sum\limits_{m,n} w_{mn}}$$
Eq. (4.14)

For each measured intensity I_m, a quantity ΔI_m, defined as the difference between the estimated and the measured intensity, is calculated:

$$\Delta I_m = \sum\limits_n A_n w_{mn} - I_m^{meas}.$$
Eq. (4.15)

To match a measured intensity I_m, each activity A_n is corrected with a factor proportional to ΔI_m:

$$A_n(new) = A_n(old) - R_p \frac{w_{mn}}{\sum\limits_n (w_{mn})^2} \Delta I_m$$
Eq. (4.16)

The correction of the activity in a pixel is thus also proportional to the contribution w_{mn} of the pixel to the measured intensity, i.e. only pixels contributing to the intensity ($w_{mn} \neq 0$) are corrected. A relaxation parameter R_p ranging from 0 to 1 is introduced in order to decrease the sensitivity for statistical fluctuations and, consequently, stabilize the reconstruction procedure.

Every pixel is corrected before the next measured intensity I_{m+1} is treated. An iteration is completed when the corrections have been performed for all measured intensities, m=1..M. The iteration procedure is repeated until the activity values have stabilized. In order to obtain pixel activities best adapted to all measured intensities, the mean value of each pixel during the last iteration is used.

Simulations performed within the frame of this work indicate that the technique to calculate the matrix coefficients is of more importance than the technique to solve the matrix equation. However, there is a possibility that an alternative reconstruction scheme may offer better properties than the ART, e.g. with respect to the capability to treat data points with low intensities.

A comparison of four algorithms for the purpose of emission tomography on individual fuel rods can be found in ref. [9]. The ART was compared to a maximum-likelihood method (ML), a maximum-entropy method and a Monte Carlo back-projection method. The results indicated that the ML

34

method, which takes into account the statistical nature of Poisson distributed intensities, generated the best reconstructions.

Another technique that may be of interest, which is similar to the ART, is the Additive Simultaneous Iterative Reconstruction Technique, ASIRT, where statistical considerations based on Gaussian statistics are taken into account [37].

The feasibility of alternative reconstruction schemes will be subject for future studies.

4.2.4   Image reconstruction

For the purpose of getting a qualitative overview of the measured assembly cross-section, an image reconstruction technique has been applied. Here, no assumptions are made regarding the fuel geometry. Homogeneous gamma-ray attenuation is assumed within the entire assembly. An image of the source distribution of the selected isotope is obtained in the reconstruction procedure. Here, the images are typically reconstructed based on 48x48 or 55x55 square-shaped pixels.

Examples of reconstructed images are presented in sections 6.4 and 7.3. These images may e.g. be used for controlling that the correct fuel type is modeled in the rod-activity reconstructions, see section 4.2.5. Furthermore, the possibility to use the images to determine the position of the assembly at each axial level will be subject for further studies. It may even be possible to analyze the images to detect if sub-bundles or individual rods are dislocated from their nominal positions.

4.2.5   Rod-activity reconstruction

For the purpose of obtaining accurate, quantitative numbers for the rod activities, the nominal geometry of the fuel assembly is explicitly taken into account when calculating the contribution coefficients. The gamma-ray attenuation through the matrix of fuel rods is modeled in detail using the expression in Eq. (4.13).

Furthermore, pixels are only assigned to the fuel pellets. The pixel pattern should preferably be selected to adapt to the typical source distribution within the rod of the isotope selected for the measurements. Some examples of pixel patterns that have been applied are shown in Figure 4.3.
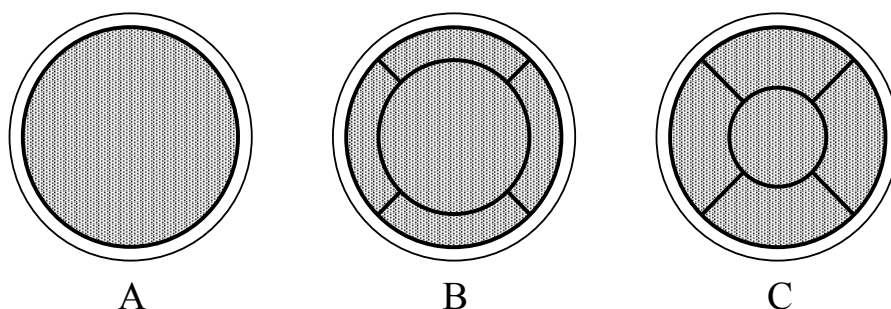
Figure 4.3. Some pixel patterns that have been applied in this thesis, involving one respectively five pixels per fuel rod, illustrated for individual rods. The zircaloy tube is also marked.

In this thesis, pixel pattern C, has mainly been used. As illustrated in Figure 4.3, this pattern involves five pixels of equal cross-sectional area, one central and four peripheral. This type of pixel pattern can adapt to the internal distribution in a fuel rod of isotopes that migrate, see section 3.1. One such isotope is ^{137}Cs, which tends to migrate towards the periphery of the rod, provided that the centerline temperature is higher than about 1500°C [28].

Furthermore, it has been shown in simulations and in measurements on a fuel model in the laboratory, that pixel patterns of types B and C imply a possibility to adapt to possible dislocations of the fuel rods. Using these types of pixel patterns, the tomographic reconstruction becomes less sensitive to the assembly position. Furthermore, a possibility to extract information about the position of each rod has been demonstrated [38].

5 Instrumentation

Initially, the tomographic method was tested in measurements on spent fuel assemblies using the poolside equipment described in section 5.3. The tests indicated that this type of measurements should preferably be performed in a fuel handling pool. Accordingly, a detector system suitable for in-pool measurements was conceived.

To gain more experience before designing the in-pool device, a laboratory device was built. It is described in section 5.4. Using this device, measurements could be performed on a fuel model to further investigate and develop the technique.

Finally, the in-pool device was constructed. It is described in section 5.5. The purpose of this device was to perform measurements on irradiated fuel assemblies with the cooling time of a few weeks.

5.1 Requirements on the equipment

For the purpose of code validation, a high level of accuracy is required in the determination of the rod-by-rod activities. In section 2.2, a relative standard deviation below 2 % was set as a desirable goal for this technique. Such a high level of accuracy sets certain requirements on instrumentation and analysis. The assumptions that were made in the derivation of Eq. (4.13) in section 4.2.2, has the following implications on the instrumentation:

- Gamma rays of a certain energy should be selected for further analysis. Contributions from gamma-ray scattering should be minimized.
- A collimator should be used, made in a highly gamma-ray attenuating material and with a slit defining the detector's field-of-view.
- The height and width of the collimator slit should be small relative to its length.
- The collimator and detector package should be positioned relative to the assembly in a two-dimensional plane (x, y), parallel to the collimator slit's main axis and perpendicular to the fuel assembly axis (z).

The first assumption implies that a gamma-ray detection system with spectroscopic capabilities should be applied so that selected gamma-ray energies can be analyzed. This is discussed in section 5.2. The other assumptions suggest that instrumentation designed according to the principles illustrated in Figure 4.1 should be applied.

The application of the tomographic measurement technique on irradiated nuclear fuel assemblies implies constraints on the instrumentation, such as safe handling of the fuel and radiation shielding of sensitive equipment. There are also constraints related to the time duration of a measurement. This is accounted for in some detail in paper IV.

5.2   Gamma-ray detection systems

A gamma-ray detection system consists of two main parts: (1) a gamma-ray detector, in which an interacting gamma quantum creates a signal, and (2) a data-acquisition system, in which the signal is registered.

5.2.1   Gamma-ray detectors

There are several types of gamma-ray detectors that can be used in this application. A discussion of the choice of detector can be found in paper IV. In this work, two types of detectors have been used:

- Scintillation detectors made of Bismuth germanate (BGO) crystals. The energy deposited by gamma quanta gives rise to photon emission in the crystal. The emitted light is converted to an electric pulse using a photo-multiplier (PM) tube.
- Semi-conducting detectors made of Germanium (Ge). The energy deposited by gamma quanta excites electrons from the valence band to the conduction band. With the aid of an applied electric field, the pairs of electrons and holes are collected and a measurable electric signal is obtained.

For both detector types, the energy deposited by a gamma quantum in the detector is thus converted to an electric pulse. The amplitude of the pulse is proportional to the deposited energy, so that an energy spectrum can be constructed.

Gamma quanta that deposit all their energy in the detector will create a full-energy peak in the spectrum. The positions of the full-energy peaks identify uniquely the isotopes involved. Examples of gamma-ray spectra, recorded on an irradiated nuclear fuel assembly using a BGO and a Ge-detector, respectively, are presented in Figure 5.1.
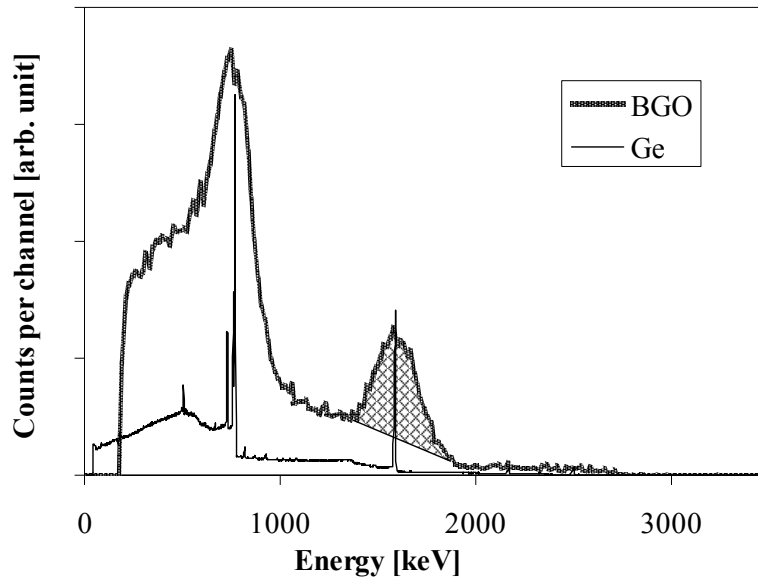
Figure 5.1. Gamma-ray spectrum of an irradiated nuclear fuel assembly, collected using a BGO detector respectively using a Ge-detector. The cooling time of the fuel was four and six weeks, respectively. The two largest full-energy peaks correspond to the decay of ^{95}Zr/^{95}Nb (757 keV / 766 keV) and ^{140}Ba (1596 keV). Analysis of the number of events in the ^{140}Ba peak by means of linear background subtraction is illustrated.

The two largest full-energy peaks in these spectra correspond to the decay of ^{95}Zr/^{95}Nb (757 keV / 766 keV) and ^{140}Ba (1596 keV). As illustrated, the energy resolution is significantly higher for the Ge-detector than for the BGO detector, which is beneficial in terms of identifying and quantifying the full-energy peaks. However, when the gamma-ray peak of interest is not disturbed by other nearby peaks in the spectrum, a lower energy resolution also be accepted. This is the case for the 1596 keV peak of ^{140}Ba in Figure 5.1. Quantitative analysis of the 1596 keV peak in the BGO spectrum by means of linear background subtraction is illustrated in the figure.

The applicability of the Ge-detector is limited by the requirement of cooling for reducing thermal noise in the detector. Furthermore, the Ge-detector is relatively expensive and bulky. Among the main advantages of the BGO detector is low cost and high intrinsic detection efficiency. It is therefore a feasible choice in applications in which its lower energy resolution can be accepted, as illustrated in Figure 5.1.

5.2.2 Data-acquisition systems

A data-acquisition system is utilized to collect and record the information from the gamma-ray detectors. The main components in a data acquisition system for spectrum collection are:

- Amplifier. Besides amplification of the electric pulse from the detector, the amplifier shapes it for further processing.
- Analog-to digital converter (ADC). The pulse amplitude is determined and converted to a digital signal.
- Multi-channel analyzer (MCA). Each pulse adds a count to a register where the memory address depends on the pulse amplitude, i.e. the deposited energy in the detector. In that way, spectra are stored of the type presented in Figure 5.1.

The data acquisition system used in the poolside instrumentation, described in section 5.3, was based on the Nuclear Instrumentation Module (NIM) standard.

Also the instrumentation used in the laboratory experiments, which is described in section 5.4, was based on the NIM standard. However, in these experiments, a single-channel analyzer (SCA) and a counter module were used instead of the ADC and MCA modules. Thus, no spectra were recorded. Instead the number of events within a certain energy interval was counted in each detector position. This simplification was motivated by the fact that only one gamma-ray energy was considered here.

Finally, in the in-pool instrumentation, described in section 5.5, a PC-card[3] offering the same functionalities as the NIM modules was utilized.

In applications involving high counting rates, it is important to keep track of the dead time of the data acquisition system. In the system used in the in-pool measurements, this was performed internally on the PC-card. However, a pulser with well-known frequency was also applied in order to perform independent evaluation of the dead time. The pulser method was also used for the poolside instrumentation.

When using the in-pool instrumentation, high counting rates were expected. The throughput of this data-acquisition system was therefore investigated, as accounted for in paper IV, showing a capability of handling input count rates exceeding 10^5 s^{-1} with minimal distortion of the energy spectrum.

5.3 Poolside equipment

The poolside equipment is installed at the interim storage for spent nuclear fuel, CLAB, in Oskarshamn, Sweden. The equipment is intended for and mainly used in gamma scanning measurements of nuclear fuel [29]. However, it was rebuilt in order to perform initial tomographic tests. The equipment is illustrated in Figure 5.2.

---

[3] MCArd 5004 from APTEC-NRC Inc.

Water   Air

Pool wall
(Concrete)

Translation

Rotation

Air

Fuel
assembly

Detector

Collimator length 1,20 m

Distance assembly-end of collimator 2,46 m

Elevator

Pool

Fuel assembly

Gamma-ray detector

Data acquisition
and computer

Collimator
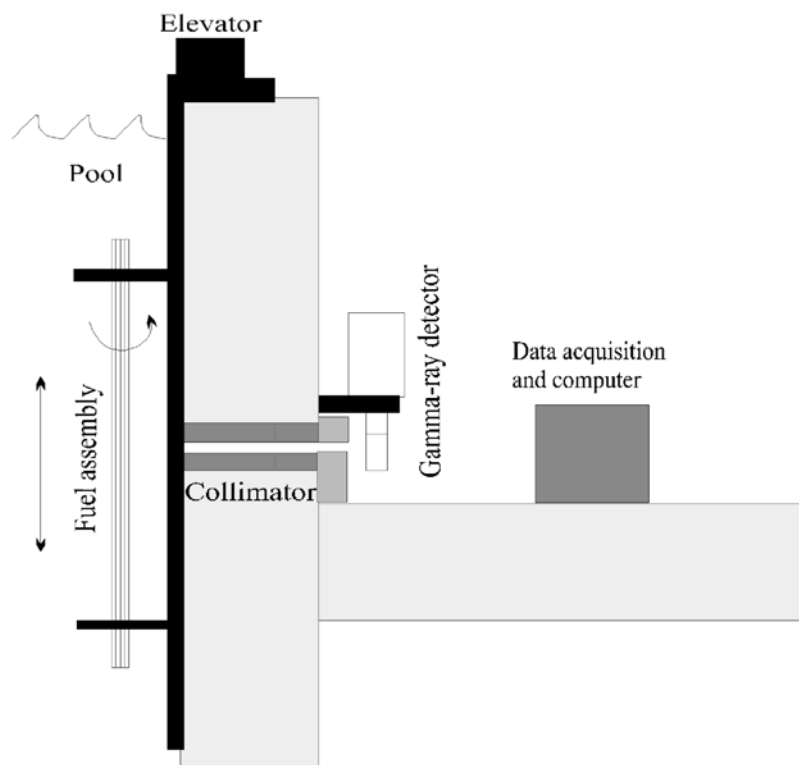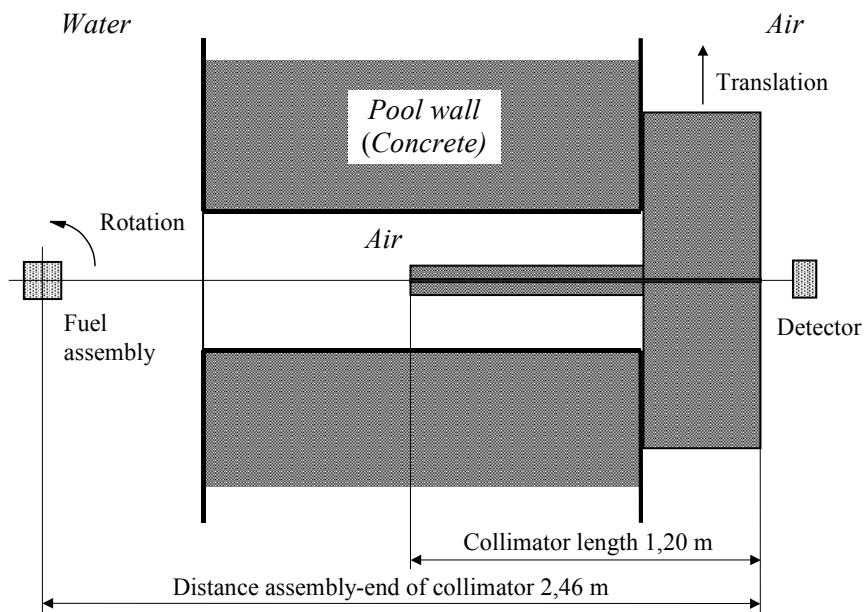
Figure 5.2. Poolside equipment. Schematic top view (above) and side view (below).

To perform the test measurements, a fuel assembly was placed in a fixture, situated to the left in Figure 5.2. The assembly could be placed in a suitable vertical position with the aid of an elevator. The fixture could be rotated 360°, allowing the radiation field to be recorded in any selected projection angle. The detector and the collimator could be translated laterally to cover the whole projection of the assembly. The width of the vertical collimator slit was 1 mm.

The detector used was a 40 % efficiency Ge-detector with an energy resolution of 1.8 keV at a gamma-ray energy of 1332 keV. A data-acquisition system based on NIM modules and a specially developed PC-software was utilized to record gamma-ray spectra.

Due to its simple design, the positioning accuracy of the poolside equipment was relatively poor. The estimated uncertainties were 1° in angular position and 1 mm in lateral position. Furthermore, the fuel assembly was not firmly attached to the fixture but could move in the order of a few millimeters.

The results of the test measurements are given paper II and in section 6.3.

5.4 Laboratory device

Based on experiences from measurements using the poolside equipment, a detector system suitable for in-pool measurements was conceived. The concept consisted of four BGO scintillation detectors in a collimator arrangement. For testing the tomographic method and, in particular, a suitable detector system, a mock-up for laboratory measurements was constructed.

A fuel model was built with a radioactive content of ^{137}Cs. The fuel rods were modeled using titanium tubes filled with granulated copper activated with ^{137}Cs. The attenuation of the gamma radiation from ^{137}Cs in these materials is roughly similar to the attenuation of the radiation from ^{154}Eu or ^{140}Ba in nuclear fuel. The rods were equipped with bottom pieces of iron and could be placed in different configurations on a magnetic table with the use of a robot. Two photographs of the device are presented in Figure 5.3.
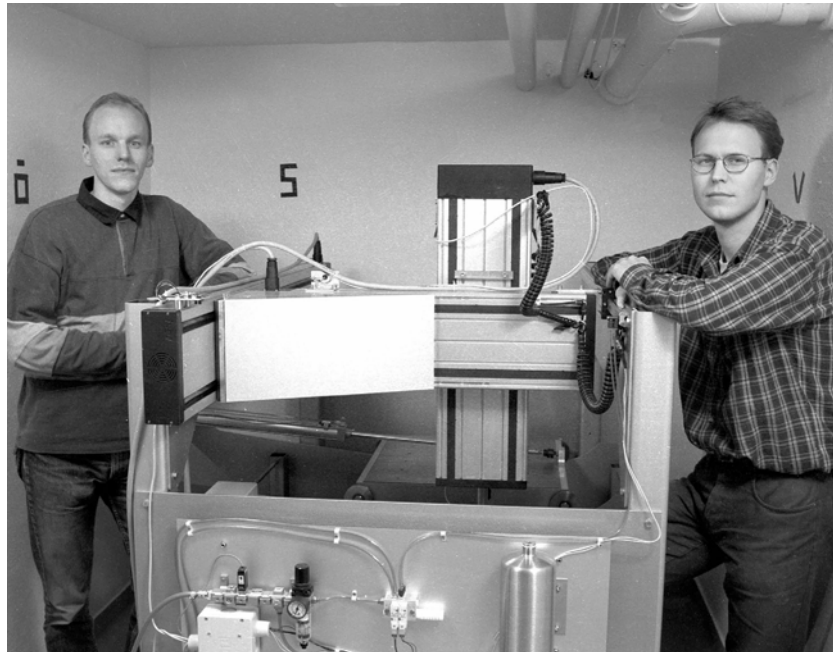
Figure 5.3. The laboratory device. A robot with three axes (above) can place the rods of the fuel model in different configurations on a magnetic table (below). A part of the collimator-detector package is seen to the left in the photograph below.

Initially, the intensity of the gamma radiation was measured from each rod separately using a Ge-detector. In such a way, it was possible to determine the relative ^{137}Cs concentration in each rod with 0.4 % accuracy.

In the investigations covered by this thesis, the rods were placed in a cross-sectional configuration similar to that of an ABB 8x8 BWR fuel assembly, illustrated in Figure 1.2. The water channel was modeled using an empty rod. The fuel channel that normally surrounds the rod bundle was not included in the fuel model.

To emulate the conditions of BWR fuel, the distribution of ^{137}Cs included a tilt over the assembly. The tilt was relatively large, ranging from 25 % lower to 24 % higher than average. The ^{137}Cs distribution is presented in Figure 5.4, normalized to an average activity of one.

	8	7	6	5	4	3	2	1
H	0.75	0.77	0.76	0.88	0.91	0.92	0.89	0.90
G	0.76	0.76	0.88	0.87	0.87	0.91	0.92	1.00
F	0.77	0.89	0.88	0.98	0.99	1.03	1.02	1.03
E	0.87	0.86	0.98	0.99	1.00	1.01	1.01	1.01
D	0.88	0.99	0.99	0.98		1.00	1.11	1.12
C	1.01	0.99	1.00	1.12	1.14	1.14	1.10	1.10
B	1.02	1.00	1.13	1.15	1.13	1.24	1.20	1.13
A	1.00	1.11	1.15	1.15	1.21	1.24	1.22	1.16
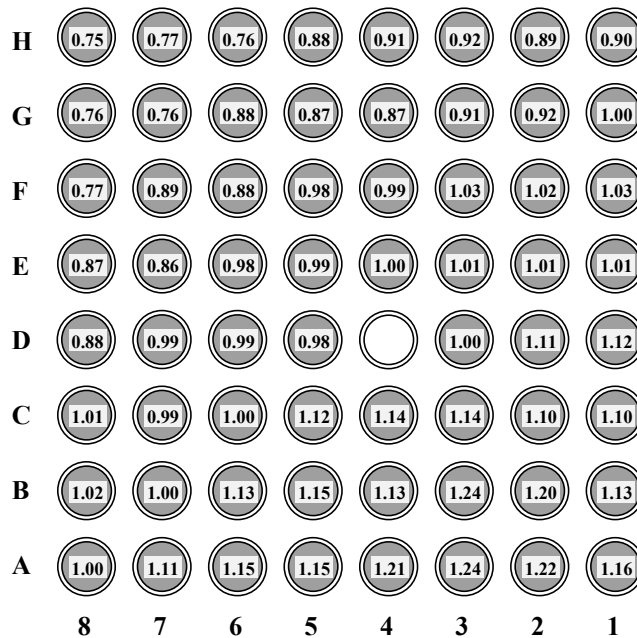
Figure 5.4. The activity configuration used in the laboratory model. The activities are normalized to a mean value of one. Position (D,4) normally contains a water channel , which was modeled using an empty rod. For the safeguards application, described in section 6.4, the ability to detect rod removal or replacement at position (E,5) was investigated. Replacement was then modeled using a non-active rod.

The measuring equipment is shown schematically in Figure 5.5. Four BGO detectors were mounted in an iron collimator. Collimator slits 30 mm high and between 1 and 3 mm wide were available. The slit length was 300 mm and the distance between the collimator opening and the assembly center was 197 mm.
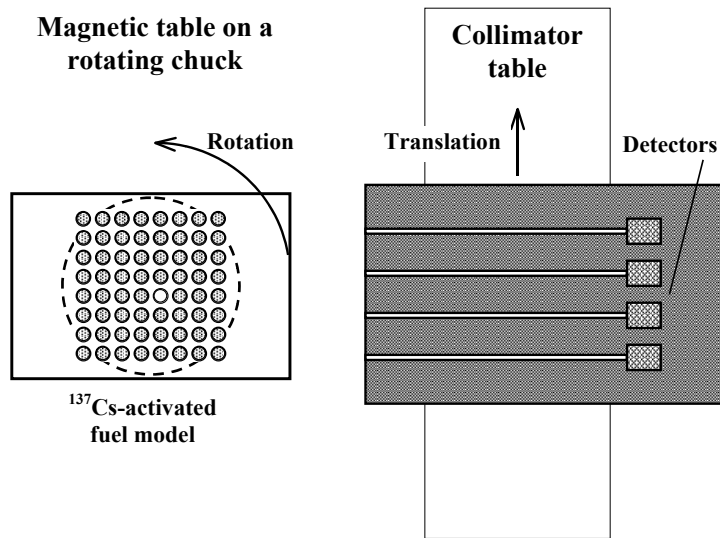
Figure 5.5. Measurement equipment of the laboratory device. Schematic view from above.

The data-acquisition system was based on NIM modules. A single-channel analyzer (SCA) was used together with a counting card for counting the events in the 662 keV full-energy peak of ^{137}Cs. A spectrum obtained in a separate measurement using an ADC module is presented in Figure 5.6, including an illustration of the lower discriminator level of the SCA.
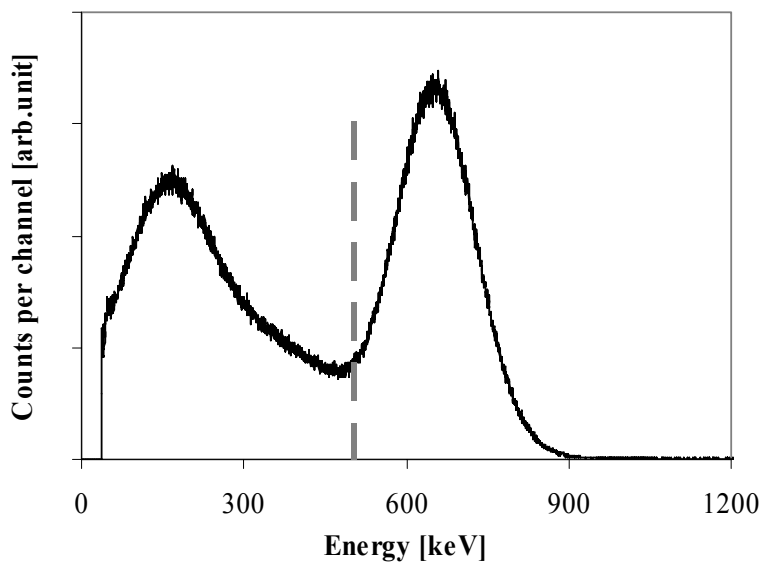
Figure 5.6. A spectrum obtained using the BGO detectors in measurements on the fuel model at the laboratory. The lower discriminator level of the SCA is illustrated.

5.5 In-pool device

Based on experiences gained from the laboratory measurements, a device was constructed for in-pool measurements on fuel assemblies with short cooling time (2-6 weeks). The main purpose of the device was to determine the pin-power distribution by measuring the 1596 keV gamma radiation emitted in the decay of ^{140}Ba. All internal instrumentation was designed within the project described in this thesis[4]. The instrumentation housing was constructed at the Forsmark NPP. The device is described in some detail in paper IV.

The design criteria are accounted for in Paper IV. Among these, it can be noted that the device was designed for a service interval of 100 h operation in the radiation field from a fuel assembly with a cooling time of 3-4 weeks. Under those circumstances, radiation doses to the device of up to 100 kGy were expected. Accordingly, radiation-resistant materials were selected and sensitive instrumentation was shielded using lead or tungsten. Furthermore, cables were cast in radiation-resistant polyurethane.

The device was intended for measurements at Swedish and Finnish NPPs. Device dimensions, as well as handling routines, are similar to those of the transport cask for spent fuel that is used in Sweden and Finland [39]. It has a diameter of 1.8 m, a height of 5.1 m and a dead weight of 30 metric tons.

To perform measurements, the device is placed at the bottom of a fuel-handling pool. A fuel assembly is placed in the axial through-channel of the device, where it is fixed during the measurements. The fuel assembly is thus continuously surrounded by a free flow of pool water, ensuring appropriate cooling of the fuel.

The device is illustrated schematically in Figure 5.7. Two photographs of the device are shown in Figure 5.8.

---

[4] The construction was performed in cooperation with Henry Andersson at Ollajvs Produktutveckling AB.

Fuel channel (waterfilled)

Fuel assembly

Collimator and detector system

Rotation table

Elevator table

Water inlet

5100

Ø1800
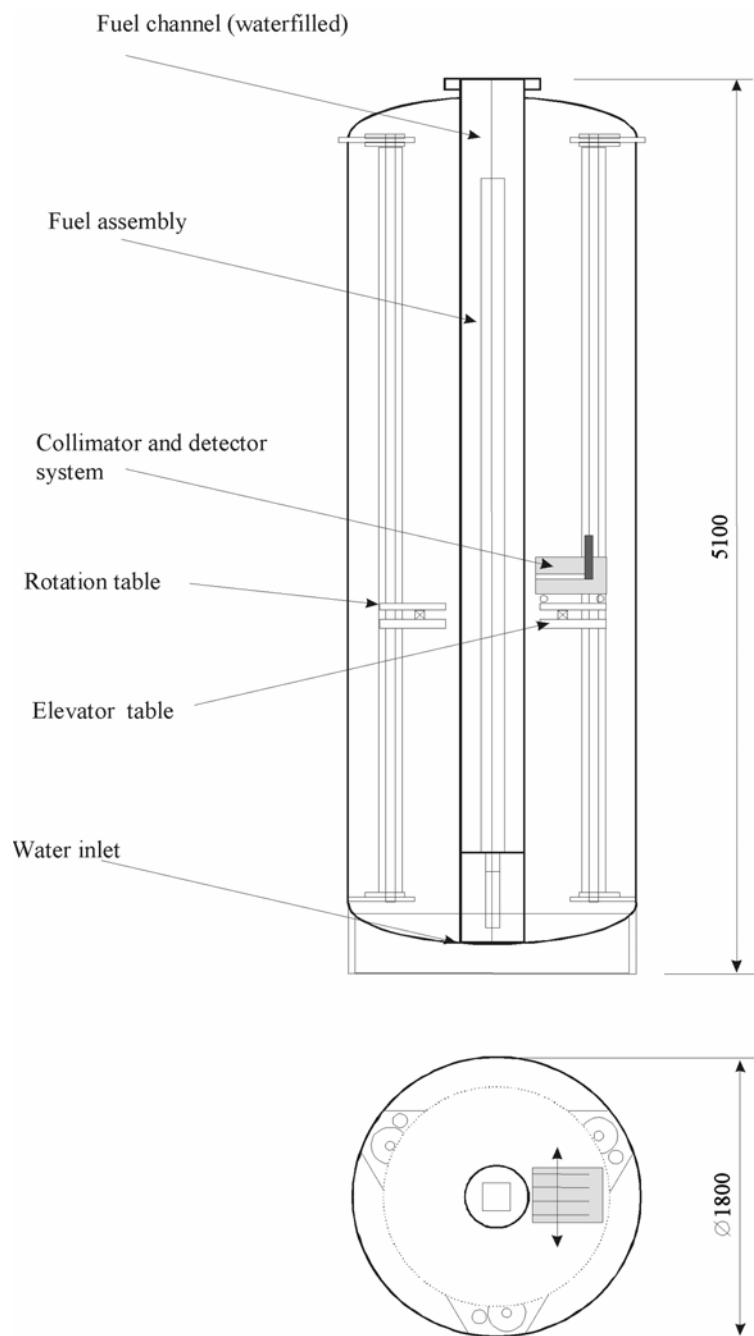
Figure 5.7. Schematic illustration of the in-pool device.
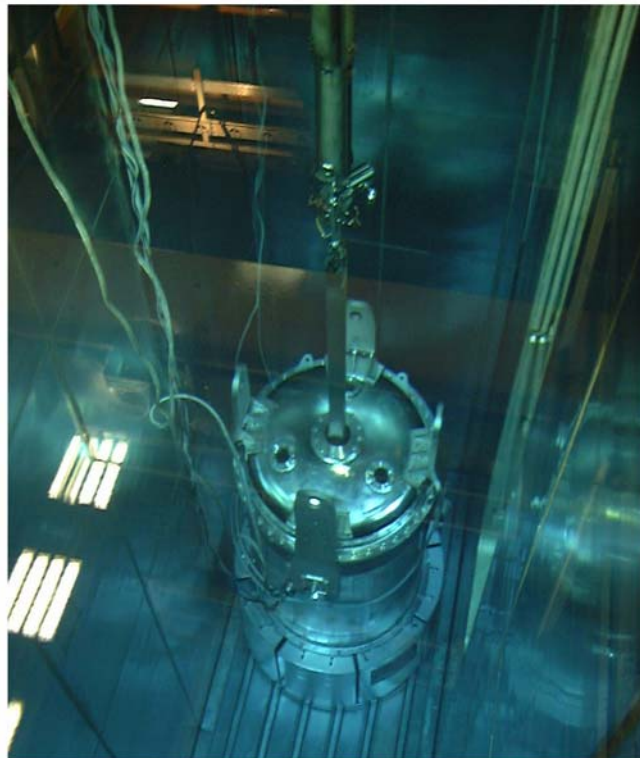
Figure 5.8. The in-pool device during transport (above) and during measurement in a fuel-handling pool at the Forsmark 2 NPP (below).

Inside the device is a supporting table for the instrumentation. Currently, the device is equipped with four BGO detectors, situated in a collimator package made of a tungsten alloy. For each detector there is a collimator slit, defining the field-of-view at the assembly. A system for transporting water through the collimator package is included in order to provide a thermally stable environment for the BGO detectors.

The BGO detectors are connected to a data-acquisition system with spectroscopic capabilities, as discussed in section 5.2.2. Gamma-ray spectra are recorded using a multi-channel analyzer and spectroscopic analysis of selected full-energy peaks can be performed on-line as well as off-line.

The collimator is primarily made for measurements on BWR fuel. However, it is constructed in modules to facilitate easy addition of extra detectors and slits for the case of measurements on PWR fuel, which has a larger cross section. Furthermore, the modular construction makes it possible to change dimensions of the collimator slits. The collimator package is shown in Figure 5.9.
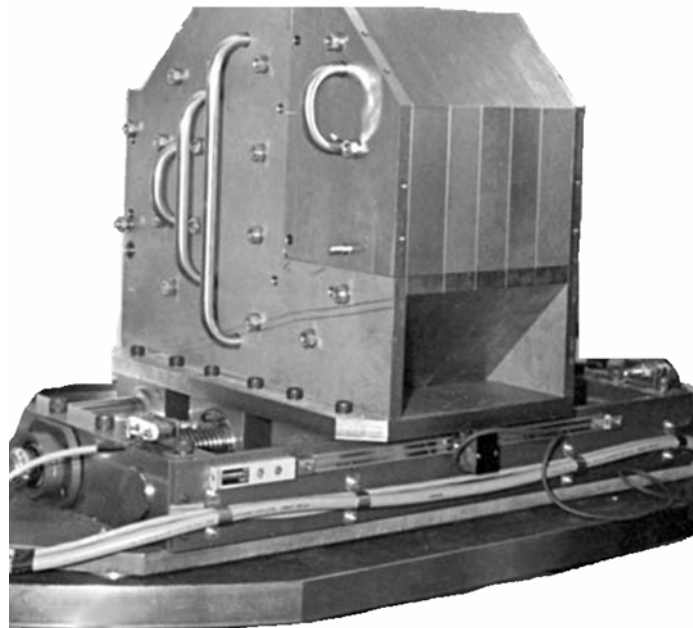
Figure 5.9. A photograph of the collimator package of the in-pool measurement device, seen from the back end. The BGO detectors are mounted inside the collimator package, which has a weight of about 750 kg. The package is mounted on a support that allows for lateral positioning. A linear encoder with an optical unit for readout of the lateral position is visible in the photograph. The collimator support is, in turn, mounted on the instrumentation table. The pipes seen at the side of the collimator package are part of the system for transporting water through the package for temperature stabilization.

The instrumentation table can be moved vertically in order to allow for measurements at different axial levels of the fuel. At each axial level, the table can be rotated and the collimator package can be laterally translated to record the radiation field in various positions relative to the assembly. The positioning along each axis is performed within 0.1° and 0.1 mm. A separate, optical system with linear encoders[5] is used for readout of the position with better than 0.01° and 0.01 mm accuracy.

It should be noted that the position of the fuel assembly relative to the instrumentation may vary, e.g. due to channel bow. The position has to be known to allow for accurate modeling in the tomographic reconstruction procedure according to section 4.2. In the measurements described in this thesis, the assembly position was determined by analyzing recorded radiation patterns. These patterns were recorded separately before the tomographic measurements were started. The accuracy of this procedure was estimated to be better than 0.1° and 0.1 mm.

---

[5] Manufactured by Heidenhain AB.

6 Results: Partial-defect verification (Papers I, II and III)

The tomographic technique offers a means to obtain information from the internal sections of a fuel assembly without requiring the assembly to be dismantled. The technique is therefore considered suitable for partial-defect verification of nuclear fuel assemblies for the purpose of safeguards, as described in section 2.1.

The applicability of the tomographic technique for this purpose has been investigated in computer simulations, described in paper I, and in measurements, described in papers II and III.

6.1 Influence of partial defects on the tomographic reconstructions

Partial defects in a fuel assembly will imply a change in the measuring conditions. First of all, a change in the activity matrix will occur, which is what the tomographic measurement intends to show. However, not only the activity matrix may change, but a change may also occur in the gamma-ray attenuation matrix. This will affect the tomographic reconstruction. Two types of partial defects can thus be recognized:

1. Replacement of fuel rods with a fuel-like material or fresh fuel. Such manipulations will only result in minor changes in the attenuation matrix or no changes at all. Tomographic reconstructions should yield the activity in such a position within the measurement accuracy.
2. Removal of fuel rods without replacement. This type of manipulation implies that the gamma radiation passing through such a position will be less attenuated than expected from the non-manipulated fuel geometry, implying relatively larger contributions from adjacent rods to the measured intensities. Consequently, the reconstructed activity in the position of a removed rod will be finite although there is no activity in such a position. Theoretically, one can expect more reliable results, i.e. a lower reconstructed activity in the position of a removed rod, when detecting higher gamma-ray energies. This is shown in paper I.

It can be noted that the latter type of manipulation would imply removal of material from the assembly, which may be revealed by controlling its weight. Thus, from a safeguards perspective, the former type of manipulation may be more difficult to detect and will require more sophisticated measurement techniques, such as tomography.

6.2 Computer simulations

Extensive computer simulations have been performed in order to investigate and develop the tomographic technique for application on nuclear fuel assemblies. For the purpose of safeguards investigations, various cases of removed or replaced rods have been simulated, as described in Paper I.

The algebraic approach that was used in the reconstruction procedure (see section 4.2.1) was also used in the simulations. However, in the simulations, the source distribution was selected and the gamma-ray intensity in the detector was obtained by summing the simulated contributions from all rods. Statistical noise was also added to the intensities in order to examine to what extent the source distribution could be reconstructed in the presence of noise.

A constant measurement time in each detector position was simulated, implying that the noise level varied with the simulated intensity in each position. Typically, the simulated number of counts was set to 10 000 in the position with the highest intensity, corresponding to a statistical uncertainty of 1 % (1 σ) in that position. It was estimated that such a level of noise would require a data-acquisition time per detector position of a few seconds.

In the simulations for safeguards purposes, various configurations of removed/replaced rods were assumed. The reconstructions were performed assuming a non-manipulated fuel geometry, in contrast to the simulations. The potential for detecting simulated manipulations under those assumptions was investigated.

An extensive account of the investigations can be found in Paper I and ref. [36]. The influence of various physical parameters was considered. Among these were:

- The number of detector positions,
- The level of statistical noise in each position,
- The collimator width.

The simulations accounted for here were performed using between 1200 and 1600 detector positions. They were performed for BWR fuel of the 8x8 type (illustrated in Figure 1.2) and for PWR fuel of the 17x17 type (illustrated in Figure 1.3).

The simulated measurement geometry is illustrated in Figure 6.1. In simulations of BWR fuel, the distance D, between the collimator and the center of the assembly, was 150 mm. For PWR fuel, D was 240 mm.
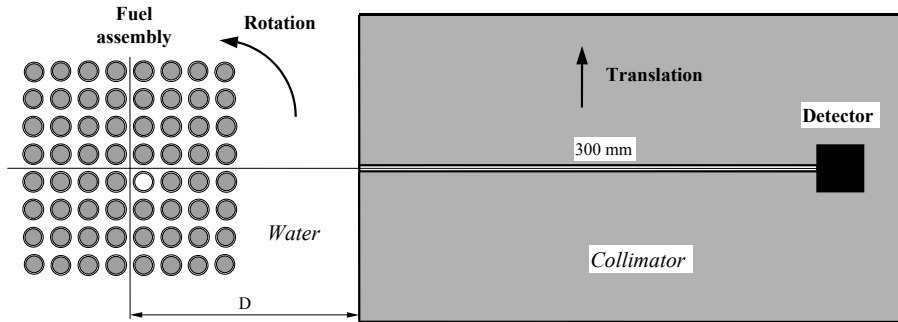
Figure 6.1. The geometry of the simulated equipment viewed from above.

Both types of partial defect discussed in section 6.1 were simulated, i.e. removal and replacement. In the simulations, removal implies that there is water in such a position. A large number of configurations of removed/replaced fuel rods are conceivable. In the simulations, the following three cases were identified as type cases:

- A. Single rods
- B. Sections of neighboring rods
- C. Rods in a chess pattern.

Two quantities were defined as measures of quality of the reconstructed activities:

- $$S = \sigma_r = \sqrt{\frac{1}{N-1} \cdot \sum_{i=1}^{N} \left(\frac{r_i - a_i}{a_i} \right)^2}$$

  The relative standard deviation between the reconstructed activity, r_i, and the simulated activity, a_i, in all positions i containing radiating fuel.

- $R = r_j/\langle r \rangle$

  The ratio of the reconstructed activity, r_j, in position j, where a fuel rod has been removed or replaced, to the average reconstructed activity, $\langle r \rangle$, in all non-manipulated positions. In cases of several manipulated rods, R_{max} denotes the maximum value of R.

In this thesis, S and R are generally expressed in percent units, i.e. the value multiplied by 100.

53

The definitions above imply that an optimal reconstruction corresponds to $R = S = 0$ %. However, due to statistical fluctuations, values of zero cannot be expected. The goal has been to find strategies to minimize S and R.

The simulations have shown that the value of S increases with an increased level of noise. However, no systematic correlation has been found between the value of R and the noise level.

6.2.1 Replacement of rods with fresh fuel or a fuel-like material

For the simulations where fuel rods were replaced with fresh fuel or a fuel-like material, the largest value of R in any position, in either BWR or PWR fuel, was about 10 %. For the simulated noise level, corresponding to 10 000 counts in the position with the highest intensity, the value of S was 2 % or better in all simulations.

The combination of accurate reconstructed activities in normal rods with reconstructed activities close to zero in replaced rods show that this type of manipulation should be possible to detect with very high confidence.

6.2.2 Removal of rods in BWR fuel

In accordance with the discussion in section 6.1, larger values of R were obtained for the case of rod removal than for replacement. Values of R_{max} and S obtained in simulations of removed rods in BWR fuel are presented in Table 6.1.

Table 6.1: Values of R_{max} and S in simulations of removed rods in BWR fuel for the ^{154}Eu and the ^{137}Cs gamma-ray energies.

Configuration of removed rods	^{137}Cs R_{max} [%]	^{137}Cs S [%]	^{154}Eu R_{max} [%]	^{154}Eu S [%]
A. Single rod (peripheral)	51.4	<2	43.6	<1.5
A. Single rod (central)	67.1	<2	48.7	<1.5
B. Inner section (15 rods)	57.7	<2	37.3	1.5
C. Chess pattern (7 rods)	59.9	4.1	43.5	3.2
C. Chess pattern (17 rods)	49.8	9.0	35.4	7.2

According to the values of R_{max} in Table 6.1, there is a significant effect of removal in all simulated cases. The highest values of R_{max} were obtained for the removal of a single, central rod.

The value of S was below 2 %, except for the chess pattern. With such a high level of accuracy for normal rods, even single rods removed from the central sections should be confidently detected, provided that the activities of the normal rods do not vary unusually much.

It could be noted that rods adjacent to the position of a removed rod were slightly affected by the disturbed geometry. This is the cause of the higher

values of S obtained for the chess patterns. However, even for the chess pattern with 17 rods removed, R_{max} was more than $5\,\sigma$ lower than the average of the normal rods.

It was also concluded that the detection capability is higher for the higher gamma-ray energy of [154]Eu than for the ^{137}Cs energy.

6.2.3   Removal of rods in PWR fuel

In agreement with the simulations on BWR fuel, the results for PWR fuel showed that the removal of a single, central rod gives rise to the highest values of R_{max}. The values of R and S were generally slightly larger than for BWR fuel. The reason is most likely the larger cross section of the PWR fuel. The values obtained for R_{max} and S are presented in Table 6.2.

Table 6.2. Values of R_{max} and S obtained in simulations of removed rods in PWR fuel.

Gamma-ray energy	R_{max} [%]	S [%]
662 keV (^{137}Cs)	90	~3
1274 keV ([154]Eu)	67	~2

The value of R_{max} for the ^{137}Cs energy was considered to be too high to allow for confident detection. However, it was concluded that highly confident detection of removed rods could be obtained in the simulations using the [154]Eu gamma-ray energy.

6.3   Test measurement on spent fuel using poolside equipment

The test measurement is described in paper II. It was performed using the equipment described in section 5.3. The assembly selected for the measurements was of the ABB 8x8 BWR type, illustrated in Figure 1.2. It had been irradiated for six power cycles in the Swedish power plant Ringhals 1. The burnup was about 36 GWd/tU. By the time of the measurements, it had a cooling time of 8 years.

The radiation field was recorded in one axial level in 3 240 detector positions, distributed over 40 angles and 81 lateral positions. In each position, the gamma-ray spectrum was recorded for 11 s. An example of such a gamma-ray spectrum is shown in Figure 6.2.
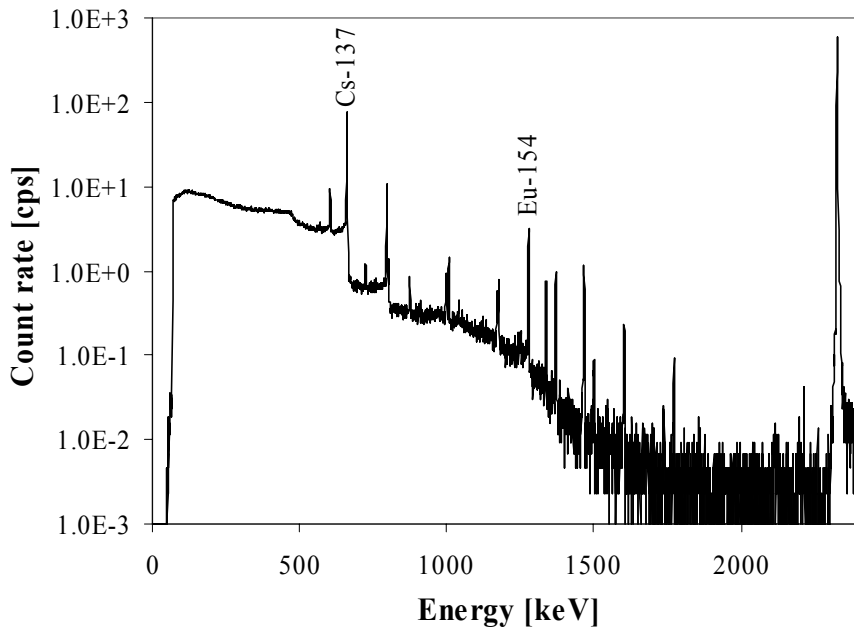
Figure 6.2. A typical spectrum from the test measurement using the poolside equipment on a BWR assembly with 8 years cooling time. The ^{137}Cs and ^{154}Eu peaks are indicated. The peak to the right is the artificial pulser peak.

Analyses were performed using both the 662 keV gamma-ray energy of ^{137}Cs and the 1274 keV energy of ^{154}Eu. Corrections for dead time were performed using the pulser method. The maximum count rate in the ^{137}Cs peak was about 500 s^{-1}, implying a maximum number of counts of about 5 500 in the position with the highest intensity. The intensity in the ^{154}Eu peak was much weaker, implying a maximum number of counts in any position of about 300.

As illustrated in Figure 1.2, the ABB 8x8 BWR fuel type normally contains 63 fuel rods and one water channel. However, this particular assembly is illustrated in Figure 6.3. Here, a fuel rod had been moved from position (E,5) to position (D,1), where it replaced another fuel rod. In position (E,5), there was an extra water channel, i.e. a water-filled zircaloy tube. The ordinary water channel is situated in position (D,4). Furthermore, this assembly was not equipped with a fuel channel.

The relative content of ^{137}Cs in each rod was calculated using the reactor analysis code SIMULATE-3 [40, 41]. The results of this calculation are also included in Figure 6.3, where the values are normalized to a mean value of 1.0. The calculated rod-by-rod content of ^{137}Cs was relatively evenly distributed, except for the positions indicated, i.e. positions (D,5), (E,4) and (D,1), showing ^{137}Cs contents considerably lower than the average value. The latter position corresponds to the fuel rod moved from position (E,5).

56

Due to the rather odd power history of the assembly, the uncertainty of the calculations was estimated to be in the order of 10 % (1 σ).

Tomographic reconstructions were performed using the rod-activity reconstruction technique, presented in section 4.2.5. In order to allow for a comparison between the measured distribution of ^{137}Cs and that calculated using the SIMULATE-3 code, as presented in Figure 6.3, a reconstruction was performed where the correct attenuation matrix was modeled, i.e. including both water channels in the center of the assembly. The reconstructed relative distribution of ^{137}Cs is presented in Figure 6.4, normalized to an average fuel rod activity of one.

The measured and the calculated values agreed with a relative standard deviation of 7.3 %. Because the estimated accuracy of the calculated distribution was relatively large (10 %), the measurement accuracy was difficult to estimate. However, it can be noted that low values were obtained in positions (E,4), (D,5) and (D,1), in agreement with the calculated distribution.

Furthermore, the ability to detect the extra water channel in position (E,5) was investigated under the assumption that no information about the replacement was available. Accordingly, a fuel rod was modeled in that position when applying the rod-activity reconstruction technique for this purpose.

Using the 662 keV gamma-ray energy of ^{137}Cs, the activity reconstructed in position (E,5), was 65 % of the average rod activity. This is in agreement with the value of R_{max} of 67 % obtained in the computer simulations of a removed, central rod, presented in section 6.2. However, when modeling a rod in position (E,5), the reconstructed activity in position (E,4) was 70 % of the average. Therefore, despite the fact that position (E,5) obtained the smallest reconstructed activity, it was not considered unambiguously distinguishable from the other rods using the ^{137}Cs energy.
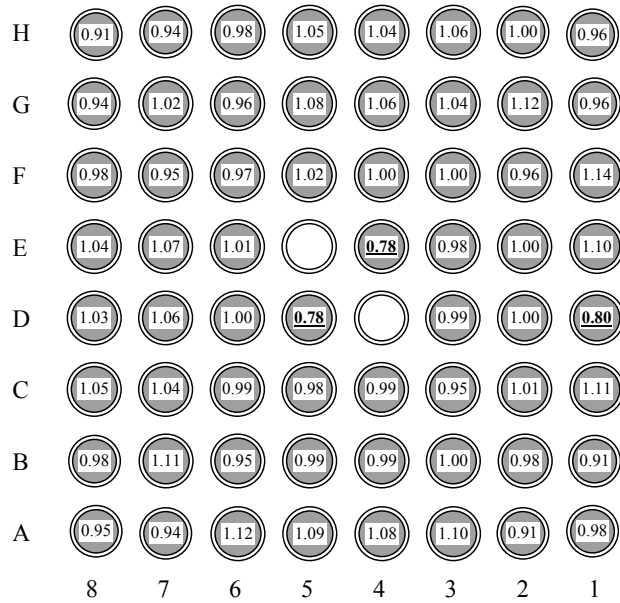
Figure 6.3. Cross section of the measured ABB 8x8 BWR fuel assembly. This particular assembly contained two water channels, in positions (E,5) and (D,4). The calculated distribution of ^{137}Cs, obtained from ref. [41] is included. The estimated uncertainty of the calculations is in the order of 10 % (1 σ).
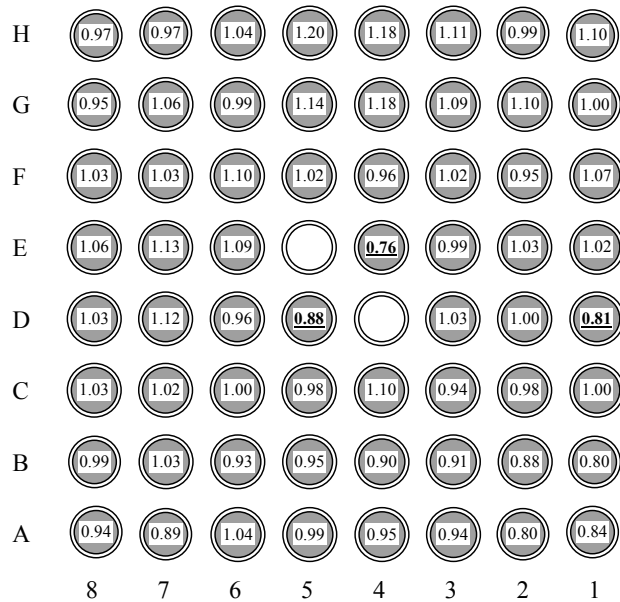
Figure 6.4. Reconstructed relative rod-by-rod distribution of ^{137}Cs. The agreement with the distribution calculated using the SIMULATE-3 code was 7.3 % (1 σ), i.e. within the estimated accuracy of the calculated distribution, which was 10 %.

The capability to detect the extra water channel was improved when using the higher gamma-ray energy of ^{154}Eu, which is illustrated in Figure 6.5. The reconstructed activity in position (E,5), was here 59 % of the average activity and the smallest value of the normal rods was 80 % of the average.

Here, no calculated distribution was available for comparison. However, the standard deviation of the obtained rod-by-rod activities was 9.9 %, position (E,5) included. The reconstructed activity in the position of the extra water channel was thus 4.2 standard deviations smaller than the average. It was clearly distinguishable from the other rods, which were all within 2.0 standard deviations from the average.
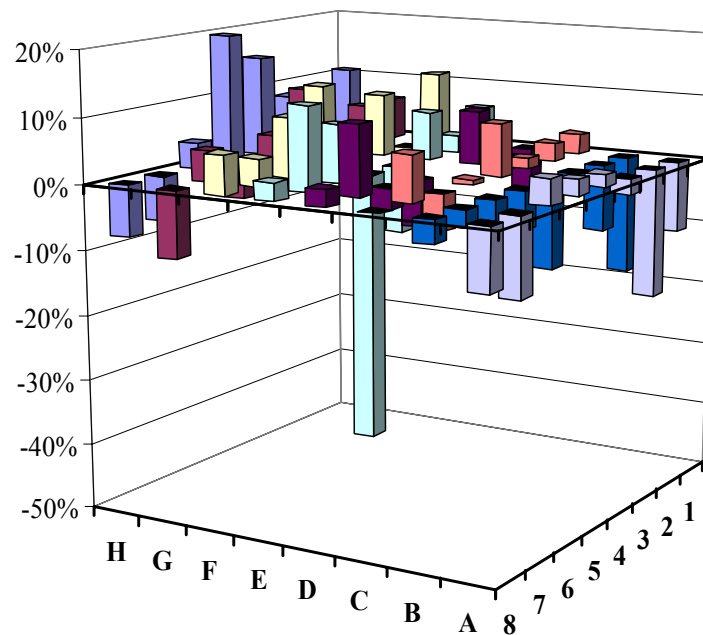
Figure 6.5. The reconstructed rod activities obtained using the 1274 keV gamma-ray energy of ^{154}Eu. Deviations from the average activity are illustrated. Note the significantly deviating value in the position of the removed rod, (E,5).

Accordingly, it was concluded that the tomographic method has a potential for partial-defect measurements, even on the single-rod level. In this set-up, the high energy resolution and high peak-to-Compton ratio of the germanium detector was crucial for accurate analysis of the relatively weak ^{154}Eu radiation.

It was also concluded that the measurements would benefit from better positioning capabilities. Finally, it can be noted that the effective data collection time in this test measurement was totally 10 hours. A closer geometry would increase the count rate in the detectors. It is estimated that the use of 8 detectors would be required to obtain a measurement time per cross section of 20 minutes.

59

6.4 Laboratory measurements on a fuel model

The instrumentation described in section 5.4 has been utilized to perform laboratory investigations of the applicability of the tomographic method for partial-defect verification. These investigations are described in paper III.

The rods of the fuel model were placed in a cross-sectional pattern similar to an ABB 8x8 BWR fuel assembly, illustrated in Figure 1.2, i.e. the fuel type that was used in the measurements performed with the poolside equipment, described in section 6.3. The water channel, situated in position (D,4), was here modeled using an empty rod. The activity configuration can be found in Figure 5.4 in section 5.4.

The ability to detect a manipulated rod in position (E,5) was investigated, both in measurements with a non-active rod in that position as well as in measurements with that position empty. A slit width of the collimator of 2 mm was selected for the measurements. The 662 keV gamma-ray intensity was recorded in 2072 detector positions distributed over 40 angles. The measurement time in each position was 10 s, resulting in a maximum number of counts in any position of about 30 000.

Based on the collected data, tomographic reconstructions of the ^{137}Cs distribution were performed using both the image reconstruction technique, described in section 4.2.4, and the rod-activity reconstruction technique, described in section 4.2.5. The purpose of the image reconstructions was to get a qualitative overview of the cross section, while the purpose of the rod-activity reconstructions was to obtain a quantitative measure of the possibility to detect a removed or replaced rod. In the latter type of reconstructions, the nominal geometry was modeled, i.e. with 63 rods and a water channel in position (D,4).

The results obtained in the measurements where the rod in position (E,5) was replaced with a non-active rod are shown in Figure 6.6. The results where position (E,5) was empty can be found in Figure 6.7.

The image reconstructions were based on 48x48 pixels. However, in order to present the images, the number of pixels was increased by applying a conventional bicubic interpolation scheme. In the images presented in Figure 6.6 and Figure 6.7, the whole range of reconstructed activities is covered. Light areas illustrate low and dark areas illustrate high activity. The results from the rod-activity reconstructions are presented as deviations from the average rod value in order to facilitate the interpretation.
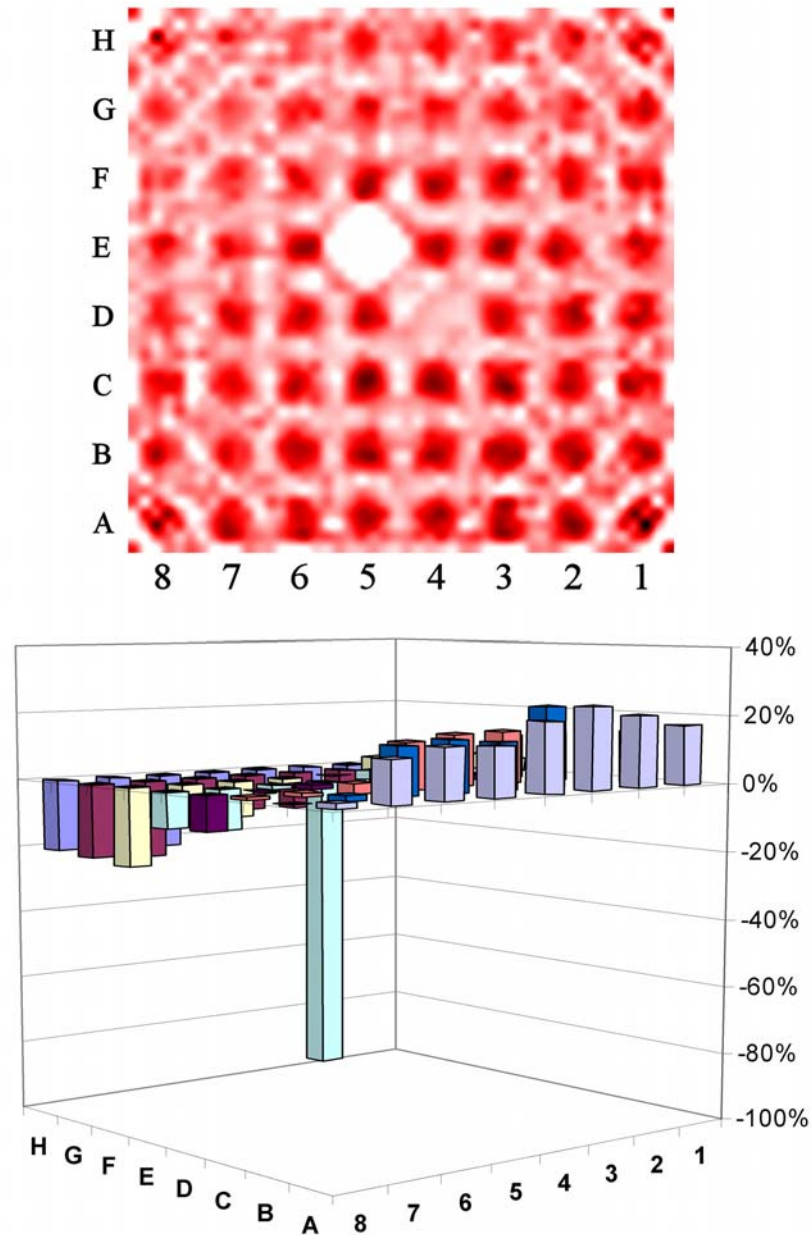
Figure 6.6. Experimentally obtained reconstructions of a fuel model with a non-active rod in position (E,5). In position (D,4), there was an empty rod, representing the water channel. In the image reconstruction (above), the whole range of reconstructed activities is illustrated, where light areas illustrate low and dark areas illustrate high activity. In the rod-activity reconstruction (below), deviations from the average rod activity are presented. The value in the position of the replaced rod is significantly smaller than the other positions. The distribution of rod activities reflects with 1.5 % accuracy (1 σ) those corresponding to the actual distribution.
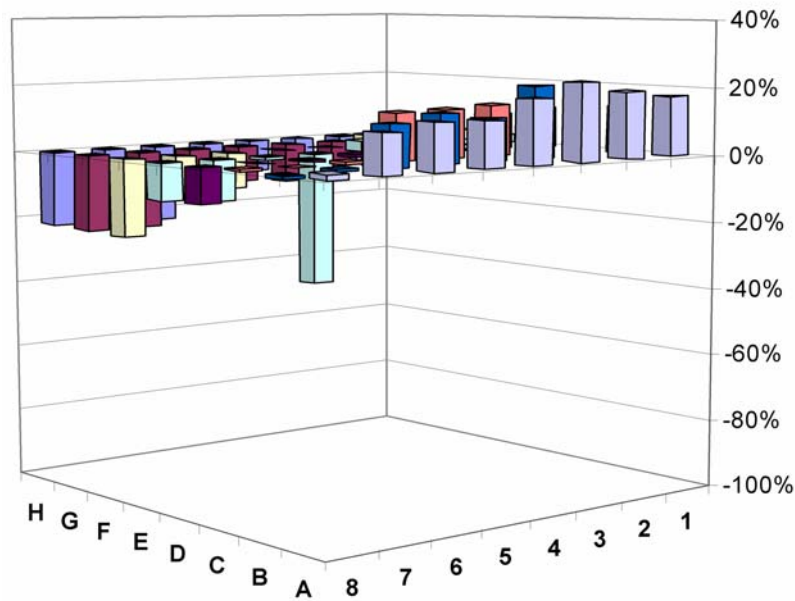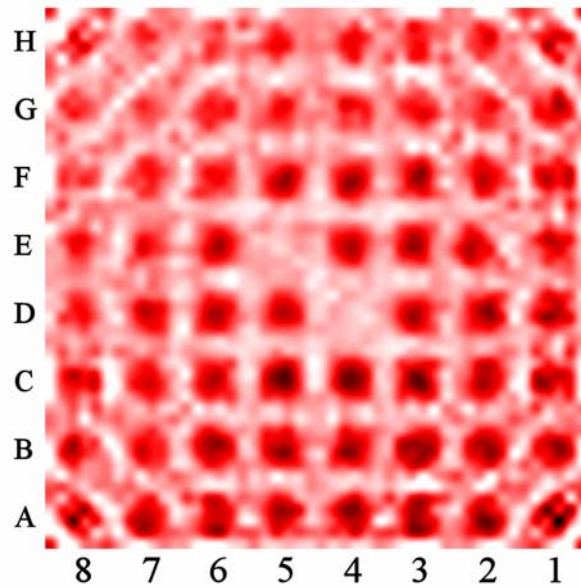
Figure 6.7. Experimentally obtained image of a fuel model where the rod in position (E,5) has been removed. In position (D,4), there is an empty rod, representing the water channel. In the image reconstruction (above), the whole range of reconstructed activities is illustrated, where light areas illustrate low and dark areas illustrate high activity. In the rod-activity reconstruction (below), deviations from the average rod activity are presented. The value in the position of the replaced rod is significantly smaller than the other positions. The distribution of rod activities reflects with 1.5 % accuracy (1 σ) those corresponding to the actual distribution.

It was considered that the purpose of the image reconstructions was achieved, i.e. to obtain a qualitative overview of the data. The following conclusions could be made by inspecting the images:

- The position of the empty rod in position (D,4), representing the water channel, can be identified in both images.
- The replacement with a non-active rod in position (E,5) is evident in the reconstructed image presented in Figure 6.6.
- Also the removal of the rod in position (E,5) without replacement is clearly visible, as illustrated in Figure 6.7. The higher background level in this case, which is similar to that of position (D,4), is in accordance with the discussion about different manipulations in section 6.1.

It can be noted that there is a relatively high level of background noise in the reconstructed images presented above in Figure 6.6 and Figure 6.7, making the fuel rods appear diffuse. A likely reason is the discriminator analysis of the spectra, illustrated in Figure 5.6. Such analysis leads to a contribution to the recorded number of counts from scattered gamma rays, which appear as a background in the spectrum under the full-energy peak. More distinct images can be expected by performing spectroscopic peak analysis involving background subtraction, which is demonstrated in section 7.3. The image quality may also be improved by increasing the number of measured angles.

In the rod-activity reconstructions, quantitative data were obtained. The ability to detect the removal/replacement of rod (E,5) could be verified:

- Accurate reconstruction of the tilted activity distribution, as presented in Figure 5.4, was demonstrated. The rod activities were reconstructed with a relative standard deviation of 1.5 %, as compared to actual activities.
- The replacement with a non-active rod in position (E,5) could be detected with high confidence, as presented in Figure 6.6. The reconstructed activity in that position was 16 % of the average. This should be compared with the smallest activity of the normal rods, which was 75 % of the average.
- The removal of the rod in position (E,5) could also be confidently detected, as presented in Figure 6.7. The reconstructed activity in that position was 60 % of the average. This was 15 % smaller than the lowest activity of the normal rods.

Because the activity in the normal rods was reconstructed with 1.5 % accuracy (1 σ), it can be concluded that both removal and replacement are detectable with very high confidence.

6.5 Conclusions and remarks

The applicability of the tomographic technique for partial-defect verification has been demonstrated. Two types of partial defects have been investigated, with the following results:

- Replacement of rods with fresh fuel or a fuel-like material.
  Highly confident detection of partial defects, even on the single rod level, has been demonstrated in computer simulations as well as in measurements using the laboratory device on a fuel model.

- Removal of rods.
  Computer simulations have indicated that confident detection of partial defects can be obtained, even on the single rod level. For BWR fuel, either the 662 keV gamma-ray energy of ^{137}Cs or the 1274 keV energy of ^{154}Eu may be used. For PWR fuel, the higher gamma-ray energy of ^{154}Eu may be required for confident detection of the removal of individual rods in central positions.

  Confident detection of the removal of a single rod from the center of a spent BWR assembly was demonstrated in a test measurement using poolside equipment. In measurements on a fuel model at the laboratory, this type of removal could also be confidently detected.

Informative images have been obtained as well as highly accurate values of the activity in non-manipulated rods. The latter property may also be useful for validating operator-declared data.

The applicability of the tomographic measurement technique has also been demonstrated on fuel assemblies with a cooling time of about 4 weeks, using the in-pool device described in section 5.5. Because all rods were present in these assemblies, partial-defect verification could not be demonstrated. However, the relative activity concentration in each rod could be determined with high accuracy, which is required for enabling the detection of removed rods. The results are covered in section 7.3.

7 Results: Validation of production codes (Papers IV and V)

Initially, the tomographic measurement technique was investigated in computer simulations with the purpose to determine its potential for safeguards purposes, see section 6.2. The results indicated that the gamma-ray source concentration in normal rods could be measured with 1-2 % accuracy (1 σ).

It was noted that such a high level of accuracy would be valuable in terms of experimental validation of production codes for core simulation, see section 2.2. A project was therefore initiated in order to develop tomographic techniques and tomographic equipment especially for the purpose of code validation, using radiation emitted in the decay of ^{140}Ba, see section 3.1.1. The project resulted in the device and the measurements that are described in Papers IV and V.

7.1 Computer simulations

The potential of the tomographic technique for accurate determination of the rod-by-rod distribution of ^{140}Ba, for the purpose of code validation, has been investigated in extensive computer simulations. The simulations were performed using the technique described in section 6.2.

The goal of the simulations was to develop the technique and to find a measuring strategy that would allow the rod-by-rod distribution of ^{140}Ba to be determined with 1 % accuracy or better. Only the BWR type of fuel was considered in these investigations.

Among the conclusions that could be made, the following was noted:

- To reach better than 1 % accuracy, the gamma-ray intensity should be recorded in more than about 2 000 detector positions.
- The measuring time should allow for more than 10 000 counts in the 1596 keV full-energy peak of ^{140}Ba in a detector position where the highest intensity is obtained.
- The position of the fuel assembly should be known with accuracy better than 0.2 mm and 0.2°.

A pixel pattern with five pixels per rod, according to pattern C in Figure 4.3, was found to be feasible. A particular benefit of such a pattern was the ability to adapt to possible dislocations of the entire assembly or individual rods, without loss of accuracy in the determination of the relative rod activity.

7.2   Laboratory measurements on a fuel model

The instrumentation described in section 5.4 was used to investigate the achievable accuracy in measurements using the tomographic method. These investigations are included in paper V.

The rods of the fuel model were placed in a cross-sectional pattern similar to an ABB 8x8 BWR fuel assembly. The activity configuration can be found in Figure 5.4 in section 5.4. The reference values, given in Figure 5.4 were obtained in initial measurements performed on each rod individually. The water channel, situated in position (D,4), was modeled using an empty rod.

The 662 keV gamma-ray intensity was recorded in 2072 detector positions distributed over 40 angles. The slit width of the collimator was 2 mm. The measurement time in each position was 10 s, resulting in a maximum number of counts in any position of about 30 000.

Tomographic reconstruction was performed based on the recorded data using the rod-activity reconstruction technique described in section 4.2.5. The reconstructed relative rod-by-rod content of ^{137}Cs is presented in Figure 7.1, normalized to an average value of one. Relative differences to the reference distribution are also included.

It can be noted that there is a systematic difference between the reconstructed distribution and the reference values. Low-activity rods situated near corner (H,8) are reconstructed to higher values and high-activity rods situated near corner (A,1) are reconstructed to lower values than the reference. This may be attributed to gamma-ray scattering, which has not been taken into account in detail.

Relative rod-by-rod distribution (values)

	8	7	6	5	4	3	2	1
H	0.77	0.78	0.78	0.90	0.91	0.91	0.90	0.90
G	0.78	0.77	0.88	0.88	0.88	0.92	0.91	1.00
F	0.78	0.88	0.89	0.98	0.99	1.02	1.02	1.03
E	0.89	0.88	0.98	1.00	1.02	1.02	1.02	1.02
D	0.89	0.98	1.00	1.01		1.01	1.09	1.13
C	1.01	1.00	1.00	1.11	1.13	1.14	1.10	1.11
B	0.99	1.01	1.11	1.13	1.12	1.20	1.19	1.14
A	1.00	1.12	1.15	1.13	1.20	1.22	1.20	1.15
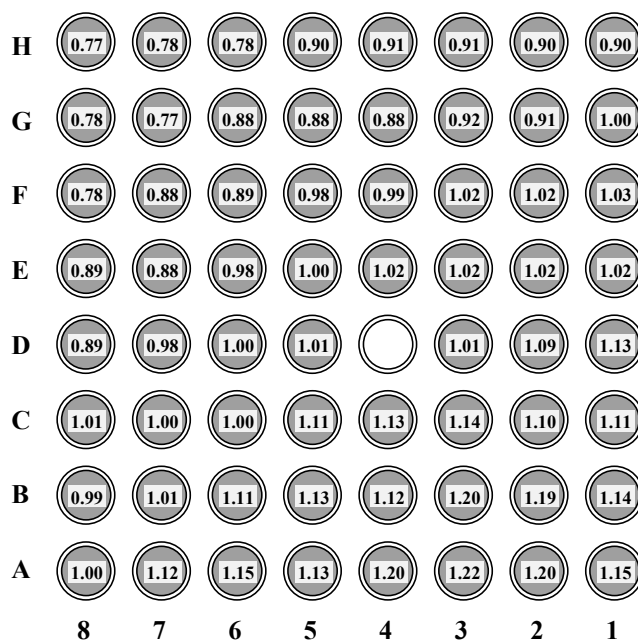
Relative differences to the reference values [%]

	8	7	6	5	4	3	2	1
H	2.1	0.7	2.0	1.8	0.8	-1.2	0.9	-0.1
G	2.5	1.3	0.2	1.3	0.8	0.8	-1.1	0.5
F	1.3	-1.6	0.3	0.5	-0.3	-1.2	-0.1	-0.1
E	2.6	1.2	-0.3	0.2	1.6	0.8	0.2	0.4
D	1.0	-0.7	0.7	2.7		1.2	-1.2	0.4
C	-0.7	0.3	-0.1	-1.4	-0.7	-0.1	0.8	0.4
B	-2.3	1.0	-1.1	-1.8	-1.1	-3.3	-0.6	0.5
A	-0.2	0.6	-0.5	-1.4	-0.7	-1.7	-1.6	-0.8

Figure 7.1. Reconstructed relative rod-by-rod distribution of ^{137}Cs in the fuel model using the laboratory equipment (above) and the relative difference to the reference value for each rod (below). The standard deviation is 1.2 %.

The standard deviation between the reconstructed distribution and the reference values was 1.2 %. This level of accuracy is considered appropriate for validation of modern production codes for core simulation.

Furthermore, the repeatability was investigated in five independent measurements. The averaged standard deviation of the measured relative rod activities in these measurements was 0.2 %. The largest standard deviation in any rod was 0.4 %.

7.3   In-pool measurements on irradiated fuel

The applicability of the tomographic technique for measurements on irradiated fuel with a cooling time of a few weeks has been demonstrated using the device accounted for in section 5.5. The device is described in some detail in Paper IV and the measurements are described in Paper V.

The distribution of ^{140}Ba was measured in two fuel assemblies of the SVEA-96S type, which is illustrated in Figure 1.2. The assemblies had been irradiated for one power cycle (~1 year). The measurements took place at the Swedish BWR Forsmark 2 during two weeks, 4-5 weeks after the revision shutdown in August 2002. The measurements were performed in axial nodes 22-25, near the assembly top. This presentation is focused on results obtained in the axial node 23. However, results of similar quality were obtained in the other nodes.

For these measurements, collimator slits were selected with a width of 1 mm, a height of 10 mm and a length of 300 mm. The distance between the collimator opening and the rotation center was 184.5 mm. Furthermore, filtering of low-energy gamma rays was accounted for by including a 30 mm lead filter in each slit.

In each axial node, data sets were recorded consisting of gamma-ray intensities in 3 400 detector positions, distributed on 40 angular and 85 lateral positions. The data collection time in each position was 5 s. The total time required to collect each data set was 3 hours. In node 23, one data set was also recorded that included 10 200 detector positions, distributed on 120 angular and 85 lateral positions. Spectroscopic analysis of the 1596 keV peak of ^{140}Ba was performed using linear background subtraction, see the BGO spectrum in Figure 5.1.

Based on the recorded data of the ^{140}Ba radiation, image reconstructions were performed according to the technique described in section 4.2.4. The purpose was to get a qualitative overview of the cross section. A reconstructed image, based on the radiation recorded in 10 200 detector positions, is shown in Figure 7.2.

This image was reconstructed using 55x55 pixels. However, in order to present the image, the number of pixels was increased by applying a conventional bicubic interpolation scheme. The same color scheme has been applied as in Figure 6.6 and Figure 6.7, i.e. the whole range of reconstructed activities is covered and light areas represent low concentration of ^{140}Ba and dark areas represent high concentration of ^{140}Ba. The four sub-bundles of the SVEA-96S assembly are clearly visible in the image.

In parallel with the measurements, the rod-by-rod distribution of ^{140}Ba was also calculated using the production code POLCA-7. The accuracy of these calculations was estimated to be 4 % (1 σ). The calculated distribution in node 23 is presented in Figure 7.3.

Figure 7.2. A reconstructed image of the ^{140}Ba distribution. The whole range of reconstructed activities is covered. Light areas represent low and dark areas represent high source concentration. The four sub-bundles of the assembly are clearly visible.

	1	2	3	4	5	6	7	8	9	10
1	0.96	1.11	1.13	1.09	1.11	1.10	1.18	1.09	1.07	0.90
2	1.12	0.73	0.90	0.93	1.07	1.06	0.91	0.86	0.84	1.04
3	1.13	0.90	1.07	0.89	1.03	1.02	0.87	1.03	0.85	1.05
4	1.10	0.94	0.89	0.91	1.10	0.99	0.98	0.86	0.88	1.13
5	1.12	1.08	1.04	1.10		1.08	1.00	1.09	1.04	
6	1.12	1.08	1.03	1.00		0.98	1.00	1.02	1.04	
7	1.20	0.93	0.88	0.99	1.09	0.98	0.88	0.85	0.89	1.12
8	1.11	0.88	1.04	0.87	1.01	1.01	0.86	1.02	0.84	1.04
9	1.09	0.86	0.87	0.90	1.11	1.03	0.89	0.85	0.97	0.95
10	0.92	1.07	1.07	1.15	1.06	1.05	1.14	1.05	0.96	0.88
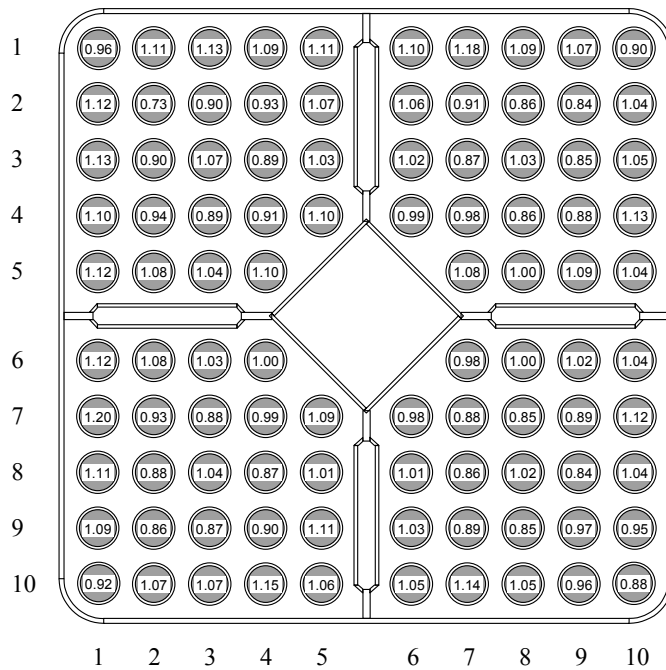
Figure 7.3. Fuel rod contents of ^{140}Ba at axial node 23, calculated using the production code POLCA-7. The values are normalized to an average of one.

69

The relative rod-by-rod content of ^{140}Ba was also reconstructed using the technique presented in section 4.2.5. The obtained distribution is presented in Figure 7.4, normalized to an average value of one. Relative differences to the calculated distribution of ^{140}Ba, obtained from the POLCA-7 code (see Figure 7.3), are also presented. The relative standard deviation between measured and calculated values is 3.1 %, i.e. within the estimated calculation accuracy of 4 %.

	1	2	3	4	5	6	7	8	9	10
1	0.87	1.09	1.14	1.08	1.11	1.09	1.19	1.10	1.05	0.83
2	1.11	0.69	0.89	0.97	1.10	1.09	0.92	0.89	0.85	1.05
3	1.14	0.91	1.09	0.89	1.04	1.00	0.87	1.03	0.86	1.08
4	1.11	0.92	0.85	0.89	1.11	0.95	0.98	0.86	0.91	1.16
5	1.15	1.10	1.01	1.07			1.04	1.02	1.13	1.07
6	1.10	1.09	1.03	0.99			0.93	0.97	1.04	1.04
7	1.23	0.93	0.89	0.98	1.07	0.97	0.85	0.81	0.89	1.15
8	1.12	0.87	1.08	0.84	1.02	0.96	0.84	1.00	0.83	1.04
9	1.09	0.87	0.90	0.91	1.15	1.07	0.92	0.85	0.98	0.93
10	0.86	1.10	1.13	1.22	1.10	1.08	1.17	1.06	0.92	0.77

	1	2	3	4	5	6	7	8	9	10
1	-9.1%	-1.9%	1.1%	-1.5%	-0.1%	-1.1%	0.7%	0.8%	-1.1%	-8.3%
2	-0.3%	-5.0%	-0.3%	3.9%	1.9%	1.9%	1.3%	2.7%	1.0%	1.0%
3	1.3%	1.7%	2.1%	0.6%	0.6%	-1.8%	0.2%	0.4%	1.1%	2.7%
4	0.7%	-1.7%	-4.3%	-2.2%	0.7%	-3.9%	-0.4%	1.0%	2.4%	2.9%
5	2.0%	1.4%	-2.2%	-2.6%			-3.5%	2.6%	3.7%	2.9%
6	-1.2%	1.2%	-0.5%	-0.5%			-5.6%	-2.7%	1.4%	0.2%
7	2.2%	0.2%	1.0%	-1.5%	-1.8%	-1.4%	-3.0%	-5.7%	0.0%	2.2%
8	0.7%	-0.9%	3.8%	-3.2%	1.5%	-4.2%	-2.1%	-1.3%	-1.9%	-0.3%
9	0.2%	1.9%	3.3%	1.1%	4.3%	3.6%	2.8%	0.6%	0.7%	-2.7%
10	-6.8%	2.9%	5.0%	6.5%	3.8%	2.0%	3.1%	1.1%	-3.8%	-12.3%

Figure 7.4. Measured fuel rod contents of ^{140}Ba at axial node 23, normalized to an average value of one (above), and the relative differences to the values obtained from the production code POLCA-7 (below). The agreement is 3.1 % (1 σ).

A systematic difference between the measured and the calculated values can be observed for the corner rods. Here, the calculated values are significantly higher than the measured values. Similar differences between measured and calculated values for corner rods have been reported in ref. [27]. However, the differences reported here are somewhat larger than in ref. [27]. A possible reason has been identified in the relatively high level of background radiation in the gamma-ray spectrum in combination with the linear background subtraction performed on the 1596-keV peak, illustrated in Figure 5.1. Alternative ways to perform the background subtraction will be subject for further studies. However, it would also be beneficial to further reduce the level of the background radiation.

It should be noted that the measuring accuracy has not yet been determined for the in-pool device. However, the repeatability was investigated in three successive measurements. The standard deviation in the determination of the relative ^{140}Ba content in individual rods ranged between 0.1 % and 2.2 % in these measurements. The averaged standard deviation was 0.8 %.

7.4 Concluding remarks

A tomographic measurement technique for experimental determination of the pin-power distribution in nuclear fuel assemblies has been developed. As compared to the conventional method, involving gamma scanning of individual fuel rods, this method does not require the fuel to be disassembled. Neither does the fuel channel have to be removed.

The purpose of the technique is to validate production codes, for which an experimental relative accuracy of 2 % or better is desirable. The potential of the present technique has been demonstrated in laboratory measurements on a fuel model, where the relative rod-by-rod content of ^{137}Cs was determined with 1.2 % accuracy.

Furthermore, a device for in-pool measurements on irradiated fuel has been constructed. The applicability of the device has been demonstrated in a measurement campaign on a BWR fuel assembly with 4 weeks cooling time. Experimentally obtained values were compared to values obtained in calculations using the POLCA-7 production code, resulting in an agreement of 3.1 % (1 σ). This was within the estimated accuracy of the POLCA-7 code of about 4 %. The repeatability, given by the averaged standard deviation of the reconstructed rod content of ^{140}Ba in three successive measurements, was 0.8 %.

The functionality of the in-pool device was satisfying. During the measurement campaign, a fuel assembly with 4-5 weeks cooling time was placed in the equipment for almost 100 hours in total. During that time, no severe failures occurred. Radiation doses to the device of between 5 kGy and

100 kGy were registered. Still, no radiation damages could be found in an ocular inspection. However, a need of improving the radiation shielding of the detectors was noted. The level of background radiation in the detectors was generally relatively high and when the instrumentation table was positioned at low axial levels of the fuel, it was unacceptably high.

The measurement time for one axial node in these measurements was about 3 hours. However, improving the data-acquisition software may shorten this time. It is estimated that a device of this type will be capable of measuring one node in 20 minutes with the same statistical properties as accounted for above, provided that it is equipped with an additional detector package. If the measuring time is to be further shortened, the addition of more detectors is possible.

A two-week long measurement campaign, performed using the suggested method, is estimated to cover 10-20 fuel assemblies in 25 axial nodes. The cost per measured fuel rod in such a campaign is estimated to be an order of magnitude lower than the conventional method.

8 Outlook

A tomographic measurement device has been built and demonstrated for the purpose of validation of production codes for reactor-core simulations. The potential of the technique has also been demonstrated for the purpose of partial-defect verification in safeguards.

However, it should be noted that the accuracy of the measurements has not yet been benchmarked. It is therefore suggested that a measurement campaign is performed, where data obtained in tomographic measurements are benchmarked versus data from gamma scanning of a limited number of individual fuel rods.

A valid benchmark of tomographically measured data is required to use these data for evaluation of the production codes. In case systematic differences are found between measured and calculated data, it may be possible to improve the production codes. Furthermore, a valid benchmark would enable the evaluation and refinement of details of the tomographic technique, such as:

- The evaluation of the count rate in the ^{140}Ba peak in the gamma-ray spectrum. Currently, a linear background subtraction technique is applied. Most likely, the measurement accuracy may be improved by including a more detailed model for the background subtraction.
- The measurement strategy. The relation between the number of detector positions used and the time for data-collection in each position should be evaluated to find an optimum. Furthermore, a pixel pattern should be selected that is appropriate for the measured activity distribution.
- The iterative algorithm used in the reconstruction procedure. Currently, the ART algorithm is used. However, alternative algorithms such as ML and ASIRT are claimed to offer better properties in the treatment of data points with low measured gamma-ray intensities. Only small differences have so far been noted between different algorithms. However, a benchmarking would offer a means to evaluate if any algorithm is superior for the current application.

Additionally, there are some areas where further development of the tomographic technique can be foreseen:

- Image analysis.
  Currently, gamma-ray projections are recorded separately in connection to the tomographic measurements in order to determine the assembly position. However, initial tests have shown the possibility to extract information of the assembly position using reconstructed images. Thus, separate measurements would not be required for positioning. Additionally, preliminary image analyses have indicated that dislocations of individual sub-bundles can be detected. In the measured SVEA-96 assembly, such angular dislocations have been indicated with a magnitude of up to about 0.8°. Such dislocations are possible within the nominal gap to the fuel channel. The analyses indicate a possibility to correct for such dislocations when modeling the fuel in the rod-activity reconstructions.
- Analysis of pixel activities within individual fuel rods.
  In addition to the image analysis technique, information of the position of an individual fuel rod may be extracted by analyzing its internal pixel values. Furthermore, information may be obtained about the internal source distribution in the rod. However, it is yet to be demonstrated if the required spatial resolution can be provided.
- More detailed physical modeling.
  In order to improve the accuracy of the technique, it is possible to include elastic and nearly elastic gamma-ray scattering in the modeling procedure.

It is also relevant to discuss properties of future devices for routine use, based on experiences gained with the instrumentation so far:

- For the purpose of partial-defect verification in connection to final repository, cooling times of the fuel in the order of 30-40 years are anticipated. Detectors and collimators should be selected with respect to the properties of the gamma-ray spectrum after such a long cooling time. Furthermore, this application requires high availability and short measuring times, which also sets demands on the instrumentation. An advantage in this application is that the device would be stationary, meaning that constraints related to weight and portability are reduced.
- For the purpose of code validation, the measuring device should allow for transportation between different power plants. The present housing of the in-pool instrumentation, described in section 5.5, is not easily transported. The possibility to change it into a lighter, transportable device, based on the same principles and instrumentation, is therefore being considered. Such a device would also include an increased number of detectors in order to shorten the measuring time. Additionally, increased shielding would be accounted for in order to further reduce the background of scattered gamma radiation in the detectors.

Acknowledgements

Of course, there are a lot of people who have helped me on the way to complete this thesis. Taking the risk of forgetting someone, I would like to mention some.

First of all, I want to express my gratitude to my supervisors, Professor Anders Bäcklin and Associate Professor Ane Håkansson, who have guided me through all the ups and downs on the way. They have openheartedly shared their experience and provided the knowledge and skills that have been required for this work.

Anders was the person who first attracted my attention to this field, when I followed his course "Experimental Techniques in Nuclear Physics" almost ten years ago. A year later, Anders announced a diploma work with the title "Experimental and theoretical investigations of tomographic methods used for determination of integrity of spent nuclear fuel" and I decided to apply. Relating it to the current thesis, one can say that I am still on the track…

Within the diploma work, Ane and I went to CLAB together to test the tomographic technique experimentally. We recorded the gamma-ray flux distribution from a spent nuclear fuel assembly in about 1000 detector positions. After spending a week in a narrow passage at CLAB, positioning the collimator manually, looking at the computer screens and saying the word "Klar" about 1000 times, the analysis of the data failed… However, I was offered a position as a Ph.D. student within the research group to redo this measurement. Apparently, the atmosphere in the group must have been nice already by then, because I accepted. I am still convinced that I did the right thing.

The next person in line to receive gratitude is Peter Jansson, who started his Ph.D. work just ahead of me. First of all, I want to acknowledge that he has contributed substantially to the content of this thesis. Without Peter's never-ending interest in computers, simulations, instrumentation, etc., it is doubtful if this work would ever have been accomplished. Additionally, Peter has contributed to the welcoming atmosphere at work, and we have also shared nice experiences outside work. I have pleasant memories from our vacations in the U.S. and from our shared physical efforts when doing the "En Svensk Klassiker".

The recent few years, two other Ph.D. students have also contributed significantly, namely Christofer Willman and Otasowie Osifo. Thank you for always giving a hand, no matter the issue; detector mounting and

Of course, being a Ph.D. student isn't just work. Among the people who have enriched my social life at ISV, I would like to mention Petter Sundberg, Joa Ljungvall, Marcus Dahlfors and Mattias Lantz. In particular, I have appreciated the "Spam foundation for social events" of Joa's and mine. Furthermore, the friends at the neighboring Department of Neutron Research, INF, should not be forgotten, among others Anders Hjalmarsson, Cecilia Johansson, Hans Henriksson, Joakim Klug and Luca Giacomelli.

Speaking of social life, I would like to mention the people of my orienteering club, IF Thor, for all enjoyable memories outside work. Also with respect to the Ph.D. studies, I have found many forerunners here.

Finally, I would like to thank my parents, Sven and Caje, for supporting and encouraging me. It has always felt natural for me to continue studying physics, and you have always supported me in this choice.

Last, but not least, the person who never seems to stop believing in me, my wife, Gunilla. You have had to put up with me coming home late many times during these years, sometimes in a good mood after finally succeeding in whatever I was doing and sometimes… not. Still, you have always been convinced that I will succeed the next day or the day after that. Thank you for always believing in me and always caring. Before closing these acknowledgements, a few words to you and our daughter, Lina: "*Tonight, I'll come home in a good mood and I'll try to be the best husband and father that I can. I love you.*"

Summary in Swedish

Tomografiska studier av bestrålade kärnbränsleelement

Denna avhandling redogör för en nyutvecklad metod för tomografiska mätningar av kärnbränsleelement samt utrustning för detta. Begreppet *tomografisk* innebär att detaljerad information kan erhållas om kärnbränsleelementens inre genom yttre mätningar, utan krav på demontering av bränslet.

Två applikationer av tekniken behandlas: *safeguards*, vilket står för kontroll att kärnämnen endast används i fredliga syften, samt *reaktordrift*, där syftet är att validera, och på sikt förbättra, de beräkningskoder som används vid kärnkraftverken. Med bättre kunnande om beräkningskodernas prestanda kan bränslet utnyttjas bättre och därmed kan man minska mängden kärnavfall.

Kärnbränsle

Den fysikaliska process som används för att generera energi inom kärnkraft är klyvning eller *fission* av tunga atomkärnor till mindre atomkärnor (fissionsprodukter). I en kärnkraftsreaktor kontrolleras fissionsreaktionen så att en kedjereaktion upprätthålls.

I svenska reaktorer innehåller reaktorhärden kärnbränsleelement nedsänkta i vatten. För att maximera effektuttaget placeras bränslet, som består av urandioxid anrikat till 2-5 % på den klyvbara isotopen Uran-235, i rör av cirka 10 mm diameter och ungefär 4 m längd. Dessa rör eller stavar buntas sedan ihop till bränsleelement. Det finns många olika typer av bränsleelement. Ett element av typen SVEA-96S, som innehåller 96 stavar, illustreras i Figur 1. I figuren illustreras även ett tvärsnitt av denna bränsletyp samt ett tvärsnitt av bränsletypen BWR 8x8, som innehåller 63 bränslestavar och en vattenkanal.
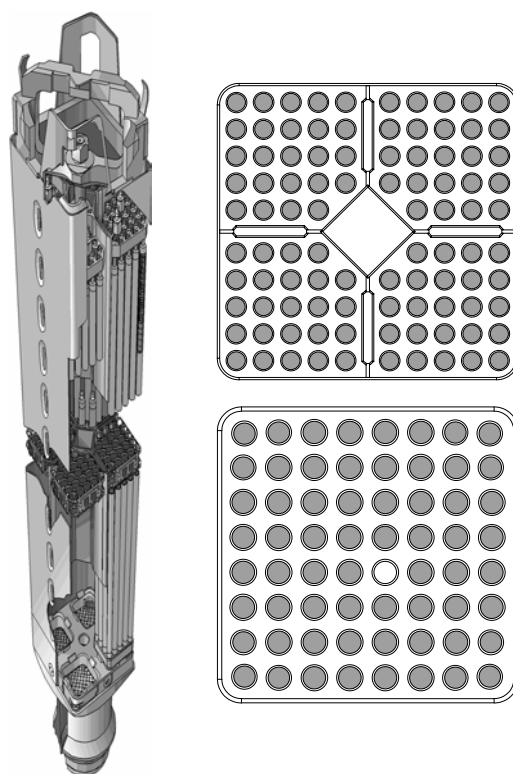
Figur 1. Till vänster illustreras ett kärnbränsleelement av typen SVEA-96S[6]. Till höger illustreras tvärsnitt av denna bränsletyp (över) samt av typen BWR 8x8 (under). Elementens längd är cirka 4 m och tvärsnitten mäter cirka 140x140 mm^2.

Driften av svenska reaktorer sker i cykler om cirka ett år. Varje år stoppas reaktorerna för revision och ungefär 20% av alla bränsleelement ersätts med nytt bränsle. De har då tillbringat 4-6 cykler i härden. Efter en förvaringstid, eller *kyltid*, av cirka ett år i bassäng vid kärnkraftverken transporteras det till SKB:s mellanlager CLAB i Oskarshamn. På CLAB kontrolleras bränslet och placeras sedan i bergrum där det skall förvaras under en kyltid om 30-40 år. Den svenska linjen är att det använda bränslet sedan skall inkapslas i stål- och kopparbehållare och förvaras under mycket lång tid, 500 meter ner i det svenska urberget.

Den tomografiska mätmetoden

Reaktorbränsle avger nästan ingen strålning innan det har varit inne i reaktorhärden, men efter att ha exponerats i reaktorhärden blir bränslet starkt radioaktivt. Främst de fissionsprodukter som har ansamlats i bränslet avger stora mängder joniserande strålning. Denna strålning kan användas för

---

[6] Bilden är publicerad med tillstånd av Westinghouse Electric Sweden AB.

diagnos av bränslet, d.v.s. att dra slutsatser om bränslets egenskaper, både omedelbart efter att bränslet har lyfts ur reaktorn och flera årtionden därefter.

Den tomografiska diagnosmetod som utvecklas ger möjligheten att erhålla noggrann information om aktiviteten av olika fissionprodukter i enskilda stavar inuti bränsleelementen, utan krav på demontering av dessa.

Metoden kräver att en stor mängd information om flödet av gammastrålning från bränslet samlas in. Detta sker med hjälp av en eller flera gammastrålningsdetektorer. En schematisk illustration av mätförfarandet återfinns i Figur 2. I illustrationen kan ett kollimatorpaket med fyra detektorer roteras till olika vinkellägen samt translateras till olika laterallägen relativt ett bränsleelement, här av typen BWR 8x8. Baserat på insamlade data om strålflödet bestäms, eller *rekonstrueras*, sedan den stavvisa aktiviteten i bränslet.
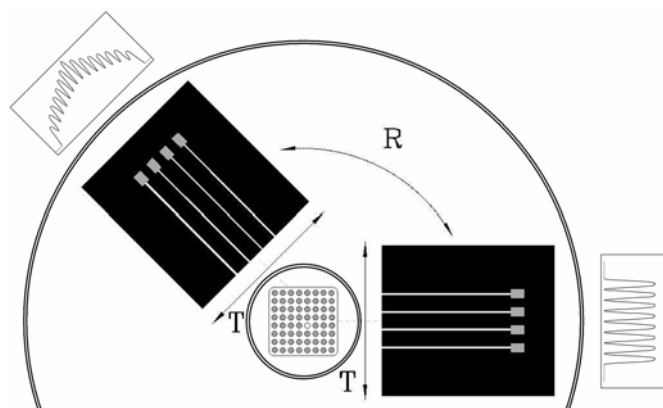
Figur 2. Principen för tomografimätningarna. Här illustreras hur ett kollimatorpaket med fyra detektorer samlar information om strålflödet från ett bränsle av typen BWR 8x8 i olika vinkellägen (R) och laterallägen (T).

En unik egenskap hos den utvecklade metoden är att bränslets kända, nominella geometri utnyttjas för stråltransportberäkningar genom bränsleelementets olika material. Detta möjliggör hög noggrannhet i aktivitetsbestämningen. Metoden har undersökts och utvecklats genom datorsimuleringar och mätningar på en bränslemodell i laboratoriemiljö. I utvecklingsfasen genomfördes även testmätningar på bränsle vid CLAB.

Baserat på den erfarenhet som erhållits under utvecklingen har utrustning konstruerats och byggts för mätning på bränsle i reaktormiljö i anslutning till revision. Bränslet har då en kyltid på 2-6 veckor, vilket innebär att mycket höga nivåer av strålning emitteras från bränslet. Detta ställer mycket höga krav på utrustningen, främst avseende systemet för datainsamling, men även avseende strålskydd av känsliga komponenter.

Några resultat redovisas i de två följande avsnitten. Resultaten innefattar dels bilder, vilka rekonstruerats för att få en överblick över det uppmätta bränslet, och dels den noggrant bestämda aktiviteten, stav för stav.

80

Kontroll av kärnbränslets integritet

Det är tekniskt mycket svårt men i princip möjligt att utvinna klyvbart material ur kärnbränsle för kärnvapenproduktion. Från det att uranmalmen bryts till det att det utbrända kärnbränslet tas ur reaktorn och förvaras eller upparbetas, löper därför en obruten kedja av kontroll och övervakning, vilket FN-organet IAEA ansvarar för. Denna verksamhet kallas kärnämneskontroll, eller *safeguards*. En viktig fråga inom safeguards är om ett kärnbränsleelements *integritet* har brutits, d.v.s. om bränslestavar har tagits ur och kanske till och med ersatts av ett likartat material.

I syfte att undersöka den tomografiska mätmetodens möjlighet att kontrollera bränslets integritet har laboratoriemätningar genomförts på en modell av bränsletypen BWR 8x8 (se Figur 1). Ett exempel på erhållna resultat redovisas i Figur 3. Här har staven i position (E,5) ersatts av en inaktiv stav. I position (D,4) återfinns normalt en vattenkanal i denna bränsletyp, vilken här har modellerats med en tom stav.
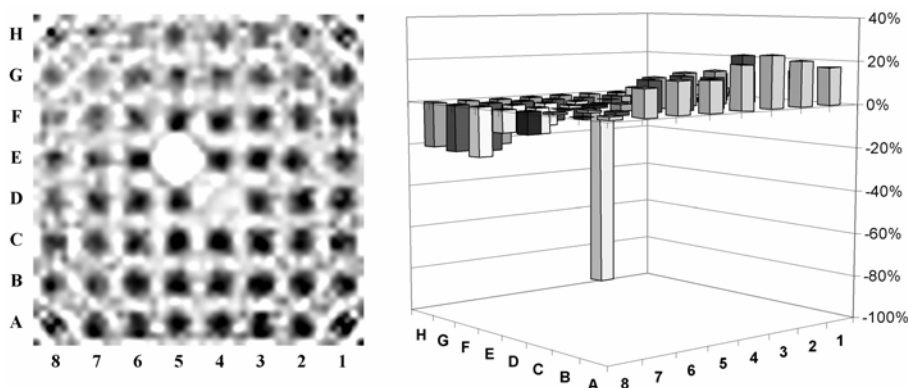
Figur 3. Resultatet av en laboratoriemätning på en modell av ett bränsleelement av typen BWR 8x8 i form av en bildrekonstruktion (vänster) och en rekonstruktion av stavaktiviteter (höger). I syfte att undersöka mätmetodens möjlighet för bestämning av bränslets integritet har staven i position (E,5) ersatts av en inaktiv stav. I position (D,4) återfinns normalt en vattenkanal, vilken här modellerats med en tom stav.

Resultatet påvisar med stor tydlighet metodens användbarhet för att detektera den här typen av integritetsbrott. I bildrekonstruktionen (vänster) kan man mycket tydligt identifiera positionen för den inaktiva staven. Även vattenkanalen framgår klart.

Den noggranna rekonstruktionen av stavvisa aktiviteter (höger), redovisas här i form av avvikelser från stavmedelvärdet. Den erhållna fördelningen, med högre aktiviteter i hörn (A,1) och lägre i hörn (H,8), återspeglar den faktiska fördelningen, vilken här bestämdes med 1.5 % noggrannhet (1σ). Den inaktiva staven erhöll i rekonstruktionen en aktivitet som var 84 % lägre än medelaktiviteten. Resultatet visar alltså att den ersatta staven kan detekteras med mycket hög konfidens.

Validering av beräkningskoder

Ett annat område där kärntekniken alltjämt utvecklas, är styrning och övervakning av processen i reaktorhärden, vilket genomförs med hjälp av olika typer av härdberäkningsprogram. Ett sådant beräkningsprogram är mycket omfattande och man kan förutsäga effektuttaget ur varje bränslestav på 25 olika höjder, motsvarande mer än 1 miljon punkter i härden.

För att säkerställa och eventuellt förbättra dessa beräkningar krävs att man experimentellt kan verifiera beräkningsresultaten. Mer detaljerad kännedom om effektfördelningen kan ge möjligheter använda bränslet mer effektivt, vilket bl.a. skulle leda till minskade mängder högaktivt avfall.

Den mätteknik som utvecklats i detta arbete har visats erbjuda möjligheter att validera de beräkningskoder som används. Detta görs genom att mäta den stavvisa fördelningen av fissionsprodukten Barium-140 i bränslet och jämföra med den fördelning som ges av härdberäkningskoderna.

Sådana mätningar har genomförts vid reaktorn Forsmark 2 på bränsle av typen SVEA-96, se Figur 1. Parallellt med mätningarna genomfördes beräkningar med härdberäkningskoden POLCA-7, med vilken stavaktiviteten av Barium-140 anses kunna bestämmas med en noggrannhet av cirka 4 %. Några resultat av mätningarna redovisas i Figur 4.

	1	2	3	4	5	6	7	8	9	10
1	-9.1%	-1.9%	1.1%	-1.5%	-0.1%	-1.1%	0.7%	0.8%	-1.1%	-8.3%
2	-0.3%	-5.0%	-0.3%	3.9%	1.9%	1.9%	1.3%	2.7%	1.0%	1.0%
3	1.3%	1.7%	2.1%	0.6%	0.6%	-1.8%	0.2%	0.4%	1.1%	2.7%
4	0.7%	-1.7%	-4.3%	-2.2%	0.7%	-3.9%	-0.4%	1.0%	2.4%	2.9%
5	2.0%	1.4%	-2.2%	-2.6%			-3.5%	2.6%	3.7%	2.9%
6	-1.2%	1.2%	-0.5%	-0.5%			-5.6%	-2.7%	1.4%	0.2%
7	2.2%	0.2%	1.0%	-1.5%	-1.8%	-1.4%	-3.0%	-5.7%	0.0%	2.2%
8	0.7%	-0.9%	3.8%	-3.2%	1.5%	-4.2%	-2.1%	-1.3%	-1.9%	-0.3%
9	0.2%	1.9%	3.3%	1.1%	4.3%	3.6%	2.8%	0.6%	0.7%	-2.7%
10	-6.8%	2.9%	5.0%	6.5%	3.8%	2.0%	3.1%	1.1%	-3.8%	-12.3%
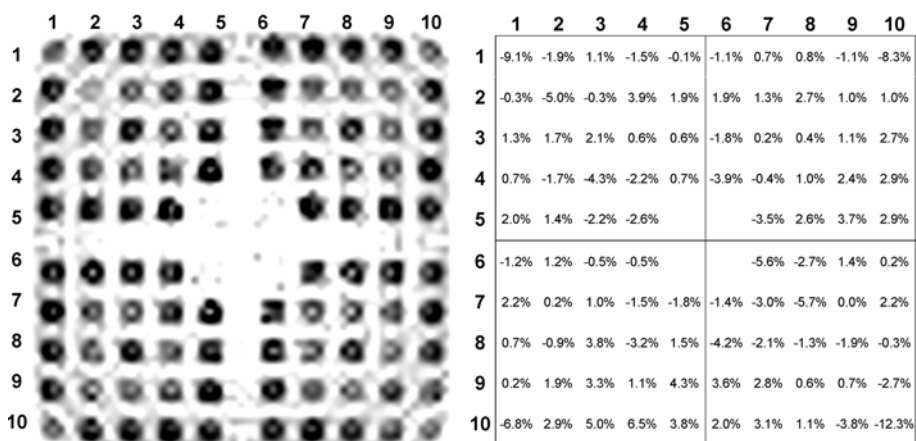
Figur 4. Några resultat av en tomografimätning på ett bränsleelement av typen SVEA-96. Tillvänster visas en bildrekonstruktion av fördelningen av fissionsprodukten Barium-140 där mörka områden betecknar hög aktivitet och ljusa områden betecknar låg aktivitet. Till höger visas avvikelser mellan rekonstruerade stavaktiviteter och den fördelning av Barium-140 som beräknats med härdberäkningskoden POLCA-7. Överensstämmelsen är 3.1 % (1 σ).

Överensstämmelsen mellan uppmätt fördelning och den fördelning som beräknats med POLCA-7 var 3.1 %, d.v.s. inom den noggrannhet som angivits för koden. Detta påvisar att den framtagna mätmetoden och utrustningen är användbar för validering av beräkningskoder.

References

1. The IAEA Power Reactor Information System (PRIS) web page. Retrieved February 18 from http://www.iaea.org/programmes/a2/
2. *Deep repository for spent nuclear fuel, SR 97 – Post closure safety*. Technical Report TR-99-06, Swedish Nuclear Fuel and Waste Management Company, SKB AB (1999).
3. The International Atomic Energy Agency, http://www.iaea.org/.
4. S. Webb, The physics of medical imaging, Institute of Physics Publishing, Bristol and Philadelphia, ISBN 0-85274-349-1 (1988).
5. A. C. Kak and M. Slaney, *Principles of Computerized Tomographic Imaging*, IEEE Press, New York, ISBN 0-7803-0447-0 (1988).
6. B. D. Sawicka, R. V. Murphy, G. Tosello, P. W. Reynolds and T. Romaniszyn, *Computed tomography of radioactive objects and materials*, Nuclear Instruments and Methods in Physics Research A, vol. 299, pp. 468-479 (1990).
7. R. Duwe and P. Jansen, *Computer tomography of barrels with radioactive contents*, Nuclear Engineering and Design, vol. 130 (1), pp. 89-102 (1991).
8. A. Alexa, T. Craciunescu, G. Mateescu and R. Dobrin, *The tomographic maximum entropy method in the 3-D analysis of nuclear fuel pins*, Journal of Nuclear Materials, vol. 218, pp. 139-142 (1995).
9. T. Craciunescu, C. Niculae, G. Mateescu and C. Turcanu, *A comparison of four tomographic methods for nuclear fuel pin analysis*, Journal of Nuclear Materials, vol. 224, pp. 199-206 (1995).
10. C. Niculae and T. Craciunescu, *On the reconstruction of the fission product distribution in nuclear fuel rods*, International Journal of Energy Research, vol. 20, pp. 999-1002 (1996).
11. F. Lévai, S. Dési, M. Tarvainen and R. Arlt; *Use of high energy gamma emission tomography for partial defect verification of spent nuclear fuel assemblies*; Report STUK-YTO-TR 56; Finnish centre for radiation and nuclear safety, STUK; Helsinki (1993).
12. F. Lévai, S. Dési, S. Czifrus, S. Feher, M. Tarvainen, T. Honkamaa, J. Saarinen, M. Larsson, A. Rialhe and R. Arlt; *Feasibility of Gamma Emission Tomography for Partial Defect Verification of Spent LWR Fuel Assemblies*; Report STUK-YTO-TR 189; Finnish centre for radiation and nuclear safety, STUK; Helsinki; (2002).
13. *IAEA safeguards criteria 1991-1995*, IAEA, Department of Safeguards, Vienna (1990).
14. *Safeguards Techniques and Equipment, 2003 Edition*, International Nuclear Verification Series No. 1 (Revised), ISBN 92-0-109403-5, IAEA, Vienna (2003).
15. Private communication, L. Hildingsson, Swedish Nuclear Power Inspectorate, SKI, March 2004.
16. K. Axell, D. Chen, A. Gerwing, L. Hildingsson, R. Keeffe, M. Larsson, B. Lindberg, R. Maxwell and F. Vinnå, *The Digital Cherenkov Viewing Device – A*

Means to Verify 40 Years Cooled Spent Fuel, Proceedings from the 25th ESARDA Annual meeting in Stockholm 13-15 May 2003.

17. P. Jansson, A. Håkansson and A. Bäcklin, *Neutronic effects of partial defects in BWR 8x8 spent fuel assemblies*, Nuclear Technology, Vol. 146 (1), pp. 58-64 (2004).

18. A. Tiitta, J. Saarinen, M. Tarvainen, K. Axell, P. Jansson, R. Carchon, J. Gerits, Y. Kulikov and Y-G. Lee, *Investigation on the possibility to use fork detector for partial defect verification of spent LWR fuel assemblies*, Report STUK-YTO-TR 191; Finnish centre for radiation and nuclear safety, STUK; Helsinki. (2002).

19. The IAEA Coordinated Technical Meeting on Spent Fuel Verification Methods in Vienna; March 3-6, 2003.

20. A. Tiitta; *NDA verification of spent fuel, monitoring of disposal canisters, interaction of safeguards and safety issues in the final disposal*; Report STUK-YTO-TR 199; Finnish centre for radiation and nuclear safety, STUK; Helsinki (2003).

21. *Benchmark Calculations of Power Distribution within Fuel Assemblies, Phase II: Comparison of Data Reduction and Power Reconstruction Methods in Production Codes*, Report NEA/NSC/DOC(2000)3, OECD Nuclear Energy Agency (2000).

22. D. Knott, *Effects of channel bow on BWR pin power distribution*, Proceedings from the 3rd ANS topical meeting on Advances in Nuclear Fuel Management, Hilton Head Island, SC, USA, October 5-8, 2003.

23. S. Jacobsson Svärd, *Changes in the pin power distribution in a nuclear fuel assembly due to geometric disturbance – simulations using the CASMO4 code*, to be published.

24. M. B. Cutrone and G. F. Valby, *Gamma Scan Measurements at Quad Cities Nuclear Power Station Unit I Following Cycle 2*, Report EPRI NP-214, Electric Power Research Institute, USA (1976).

25. B. Grapengiesser and I. Matsson, *Measurements on Fuel Assemblies from Leibstadt for Determination of Relative Power Distribution*, Report BUC 97-048, ABB Atom AB, Sweden (1996).

26. I. Matsson and B. Grapengiesser, *Developments in Gamma Scanning of Irradiated Nuclear Fuel*, Applied Radiation and Isotopes, vol. 48 (10-12), pp. 1289-1298 (1997).

27. J. J. Casal, J. Krouthén and M. Albandea, *Reliable tools to model advanced SVEA fuel designs*, Proceedings from the 3rd ANS topical meeting on Advances in Nuclear Fuel Management, Hilton Head Island, SC, USA, October 5-8, 2003.

28. S. T. Hsue, T. W. Crane, W. L. Talbert ,Jr and J. C. Lee, *Nondestructive Assay Methods for Irradiated Nuclear Fuels*, Report LA-6923 (ISPO-9), Los Alamos National Laboratory (1978).

29. A. Håkansson and A. Bäcklin, *Non-destructive assay of spent BWR fuel with high-resolution gamma-ray spectroscopy*, Report TSL/ISV-95-0121, ISSN 0284-2769, Dept. of Radiation Sciences, Uppsala University (1995).

30. G. Pfennig, H. Klewe-Nebenius and W. Seelmann-Eggebert, *Karlsruher Nuklidkarte, 6th edition 1995, revised reprint 1998*, Forschungszentrum Karlsruhe GmbH, ISBN 3-92-1879-18-3 (1998).

31. T. R. England and B. F. Rider, *Evaluation and Compilation of Fission Product Yields 1993*, Report LA-UR-94-3106, ENDF-349, Los Alamos National Laboratory (1994).

32. LBNL Isotopes Project, Fission Home Page. Retrieved February 25, 2004, from http://ie.lbl.gov/fission.html

33. P. Jansson, *Studies of Nuclear Fuel by Means of Nuclear Spectroscopic Methods*, Acta Universitatis Upsaliensis, Comprehensive Summaries of Uppsala Dissertations from the Faculty of Science and Technology 714, Uppsala, ISBN 91-554-5315-5 (2002).
34. T. Inouye, K. Kose and A. Hasegawa, *Image reconstruction algorithm for single-photon-emission computed tomography with uniform attenuation*, Physics in Medicine and Biology, vol. 34 (3), pp. 299-304 (1989).
35. L. A. Kunyansky, *A new SPECT reconstruction algorithm based on the Novikov explicit inversion formula*, Inverse Problems, vol. 17, No. 2, pp. 293-306 (2001).
36. S. Jacobsson, A. Håkansson, C. Andersson, P. Jansson and A. Bäcklin, *A Tomographic Method for Verification of the Integrity of Spent Nuclear Fuel*, ISSN 1104-1374, ISRN SKI-R--98/17--SE, Swedish Nuclear Power Inspectorate, SKI, Stockholm (1998).
37. T. Yokoi, H. Shinohara, T. Hashimoto, T. Yamamoto and Y. Niio, *Implementation and Performance Evaluation of Iterative Reconstruction Algorithms in SPECT: A Simulation Study using EGS4*, Proceedings of the Second International Workshop on EGS, Tsukuba, Japan, August 2000.
38. S. Jacobsson Svärd and M. Troeng. To be published.
39. *Certificate for transport cask TN 17/2*, No. S/40/B(U)F-85 (Rev. 8), Swedish Nuclear Power Inspectorate, SKI (2002).
40. *SIMULATE-3. Advanced three-dimensional two-group reactor analysis code*, Report STUDSVIK/SOA - 95/15 - REV 0.
41. E. Kurcyusz, *Ringhals 1- Stavutbränningsdata för gammascannad patron 8341*, Report 60/97, Vattenfall Fuel AB, Stockholm (1997).

Acta Universitatis Upsaliensis

Comprehensive Summaries of Uppsala Dissertations
from the Faculty of Science and Technology

Editor: The Dean of the Faculty of Science and Technology

A doctoral dissertation from the Faculty of Science and Technology, Uppsala University, is usually a summary of a number of papers. A few copies of the complete dissertation are kept at major Swedish research libraries, while the summary alone is distributed internationally through the series *Comprehensive Summaries of Uppsala Dissertations from the Faculty of Science and Technology*. (Prior to October, 1993, the series was published under the title "Comprehensive Summaries of Uppsala Dissertations from the Faculty of Science".)